
ON THE $PM_{2.5}$ – MORTALITY RELATIONSHIP: A BAYESIAN DYNAMIC MODEL FOR SPATIO-TEMPORAL CONFOUNDING

Carlo Zaccardi

Department of Economics
University G. d'Annunzio of Chieti-Pescara
Pescara, Italy
carlo.zaccardi@unich.it

Pasquale Valentini

Department of Economics
University G. d'Annunzio of Chieti-Pescara
Pescara, Italy

Luigi Ippoliti

Department of Economics
University G. d'Annunzio of Chieti-Pescara
Pescara, Italy

Alexandra M. Schmidt

Department of Epidemiology, Biostatistics and Occupational Health
McGill University
Montréal, Canada

Abstract

Spatial confounding, often regarded as a major concern in epidemiological studies, relates to the difficulty of recovering the effect of an exposure on an outcome when these variables are associated with unobserved factors. This issue is particularly challenging in spatio-temporal analyses, where it has been less explored so far. To study the effects of air pollution on mortality in Italy, we argue that a model that simultaneously accounts for spatio-temporal confounding and for the non-linear form of the effect of interest is needed. To this end, we propose a Bayesian dynamic generalized linear model, which allows for a non-linear association and for a decomposition of the exposure effect into two components. This decomposition accommodates associations with the outcome at fine and coarse temporal and spatial scales of variation. These features, when combined, allow reducing the spatio-temporal confounding bias and recovering the true shape of the association, as demonstrated through simulation studies. The results from the real-data application indicate that

the exposure effect seems to have different magnitudes in different seasons, with peaks in the summer. We hypothesize that this could be due to possible interactions between the exposure variable with air temperature and unmeasured confounders.

Keywords: Air pollution; Bayesian; Dynamic generalized linear model; Mortality; Non-linearity; Spatio-temporal confounding.

1 Introduction

Air pollution is a major environmental risk factor and undermines public health, causing a wide range of health problems, including premature deaths. To date, there is a very rich literature demonstrating the short- and long-term consequences of air pollution on health outcomes (see, e.g., [Dominici et al. \(2002\)](#), [Janes et al. \(2007\)](#), [Zeger et al. \(2008\)](#), [Greven et al. \(2011\)](#), [Dai et al. \(2014\)](#), [Di et al. \(2017\)](#), [Wu et al. \(2020\)](#), [Brunekreef et al. \(2021b\)](#), [Renzi et al. \(2021\)](#), [Dominici et al. \(2022\)](#), [Gamerman et al. \(2022\)](#), [Requia et al. \(2024\)](#)).

Within the ecological regression framework, one of the challenges encountered is the determination of the shape of the exposure–outcome relationship, which is commonly assumed to be constant and linear. We say that the relationship is linear if the exposure enters linearly in the specification of the link function. However, if this assumption is violated, misspecification bias would result. We acknowledge that all models are inherently flawed, but some of them are so misspecified that they can lead to incorrect inferential statements ([Gelman and Shalizi, 2013](#)).

In this paper, the ultimate goal is to correctly evaluate the short-term association between particulate matter with a diameter less than $2.5\mu\text{m}$ ($\text{PM}_{2.5}$) and all-cause mortality. The data span the period between 2018 and 2022 and are available for each health district of two Italian regions (see Section 2). We argue that the assumption of a constant and linear effect can be unrealistic for several reasons. The physical properties and chemical composition of the PM mixture may vary in time and space, as they are influenced by meteorological conditions, human activities, and the morphology of the study region ([Chen et al., 2013](#), [Masselot et al., 2022](#), [Peng et al., 2005](#)). Temperature and sunlight, for example, can improve the photochemical reactions that produce secondary aerosols ([Chen et al., 2013](#), [Peng et al., 2005](#)). Exceptional events such as sand storms ([Chen et al., 2013](#)) and wildfires ([Zhou et al., 2021](#)) cause an increase in the concentration of hazardous particles, so they can modify the association with the outcome. Human activities, such as traffic, industrial production, domestic heating, and air conditioning, change throughout the year, so they may also affect the concentration and the composition of pollutants ([Chen et al., 2013](#), [Kelly and Fussell, 2012](#), [Masselot et al., 2022](#), [Peng et al., 2005](#)). The physiological response to air pollution may also vary by season, as extreme temperatures may increase a person’s susceptibility to PM effects ([Bergmann et al., 2020](#), [Li et al., 2017](#), [Peng et al., 2005](#), [Roberts, 2004](#)). Finally, during the summer people spend more time outdoors or have windows open, and this increased natural

ventilation may enhance people’s exposure to air pollutants and reduce the exposure measurement error (Bergmann et al., 2020, Peng et al., 2006, Roberts, 2004, Stafoggia et al., 2008).

To account for the potential non-linearity of the exposure–outcome relationship, various strategies are available. An exposure-response function is often estimated (see, among others, Brunekreef et al., 2021b, Cork et al., 2023, Dominici et al., 2022, Renzi et al., 2021). Alternatively, it would be appropriate to specify a model that incorporates the inherent spatial or temporal variations of the exposure effect (Gelfand et al., 2003). Here, we focus on the temporal evolution of the impact of $\text{PM}_{2.5}$ on human health. By explicitly modeling the temporal variations in the coefficients, we can analyze whether the strength of the relationship between $\text{PM}_{2.5}$ and health outcomes have changed over different time periods. Furthermore, the temporal dynamic of the exposure effect allows investigating the influence of various factors that have emerged since 2020, such as lockdowns, the use of facial masks, physical distancing and social restrictions. These measures have significantly altered people’s habits and interactions with the environment, potentially affecting the relationship between $\text{PM}_{2.5}$ exposure and health outcomes.

Time-varying coefficients models (TVCMs) have been previously considered in the literature. For example, the exposure effect is modeled either as a periodic function (Chen et al., 2013, Peng et al., 2005) or as a season-specific step function (Dai et al., 2014, Klompmaker et al., 2023). Moreover, Chiogna and Gaetan (2002) and Lee and Shaddick (2008) employ dynamic generalized linear models (DGLMs; West and Harrison, 1997) when analyzing the relationship between air pollution and mortality with time-series data.

A second major challenge in ecological regression models relates to the exposure effect being influenced by several confounders, that is factors associated with both the exposure and the outcome variables. Although information on some of these confounders is available, such as meteorological variables, it is likely that others are unmeasured or difficult to quantify, such as influenza epidemics or changes in population structure (Peng et al., 2006). If the model does not correctly account for unmeasured confounding, the estimator of the exposure effect is biased. We denote this situation as *spatio-temporal confounding*. More specifically, we extend the notion of spatial confounding (Paciorek, 2010) to the spatio-temporal set up.

Despite the complexity of this problem, just few authors have recently proposed approaches that explicitly account for spatio-temporal confounding. For instance, Reich et al. (2021) discuss extensions of causal inference methods. Prates et al. (2022) propose the transformed multivariate Gaussian Markov random field model (TMGMRF), an extension of the approach by Prates et al. (2015), where Poisson intensities or Bernoulli rates are modeled directly and without the need of a link function. A copula structure captures the spatio-temporal dependence and guarantees the disentanglement between fixed and random effects, hence their model should be able to control for confounding bias. A spatio-temporal linear model is considered by Adin et al. (2023), where the random effects are orthogonalized with respect to the fixed effects: in other words, this work extends the restricted spatial regression model (RSR; Hodges and Reich, 2010, Reich et al., 2006). In

all these approaches, however, the exposure–outcome association is always assumed to be constant and linear.

A comprehensive data-driven approach that can capture the temporal dynamics of the exposure effect while simultaneously controlling for spatio-temporal confounding is still lacking. To tackle both problems, we propose a Bayesian DGLM, which has several advantages. First, it is able to approximate any smooth function of time (Gamerman and Lopes, 2006, Granger, 2008), hence the proposed model should not be affected by misspecification bias. Second, the proposed approach can be seen as a generalization of other methods in the literature. For example, the approaches by Chen et al. (2013) and Peng et al. (2005) cannot account for exceptional events such as the outbreak of the SARS-CoV-2 pandemic. In addition to this issue, the models proposed by Dai et al. (2014) and Klompmaker et al. (2023), among others, implicitly assume the possibility of abrupt changes. However, the latter ones are unlikely in practice, because the exposure effect depends, for example, on meteorological conditions and on human activity patterns that change gradually over time (Bhaskaran et al., 2013, Peng et al., 2005). In contrast, the proposed model is able of overcoming both drawbacks, thanks to the ability of DGLMs to capture gradual changes and to emphasize both seasonal and non-systematic variations (Bitto and Frühwirth-Schnatter, 2019, Lütkepohl, 2005, Petris et al., 2009).

A third major advantage of the proposed approach is that, following Greven et al. (2011) and Janes et al. (2007), the exposure effect is decomposed into two orthogonal components, each describing the (non-linear) association with the health outcome at a different scale of variation. This decomposition should help to distinguish the effect of interest from that of unmeasured confounding factors. Finally, the time-varying spatial-specific intercepts in our specification should allow capturing seasonal and trend components due to the unmeasured confounders.

This paper is organized as follows. Section 2 offers a brief description of the data that motivated this study and presents preliminary analyses using competing approaches. Sections 3 and 4 provide detailed information on the proposed model and on the inferential procedure, respectively. In Section 5, a simulation study is conducted to investigate the ability of the proposed approach in controlling for spatio-temporal confounding when the true association is known. The results from the real-data application are analyzed in Section 6. Finally, Section 7 provides a discussion.

2 Motivation

This paper analyzes the association between daily $\text{PM}_{2.5}$ concentrations and all-cause mortality counts among the elderly (i.e. people aged 65 or more) in Piemonte and Lombardia regions (Italy) between 2018 and 2022. In this Section, after describing the dataset, we emphasize the importance of capturing the temporal dynamics of the regression coefficients, an aspect that is not adequately addressed by existing approaches.

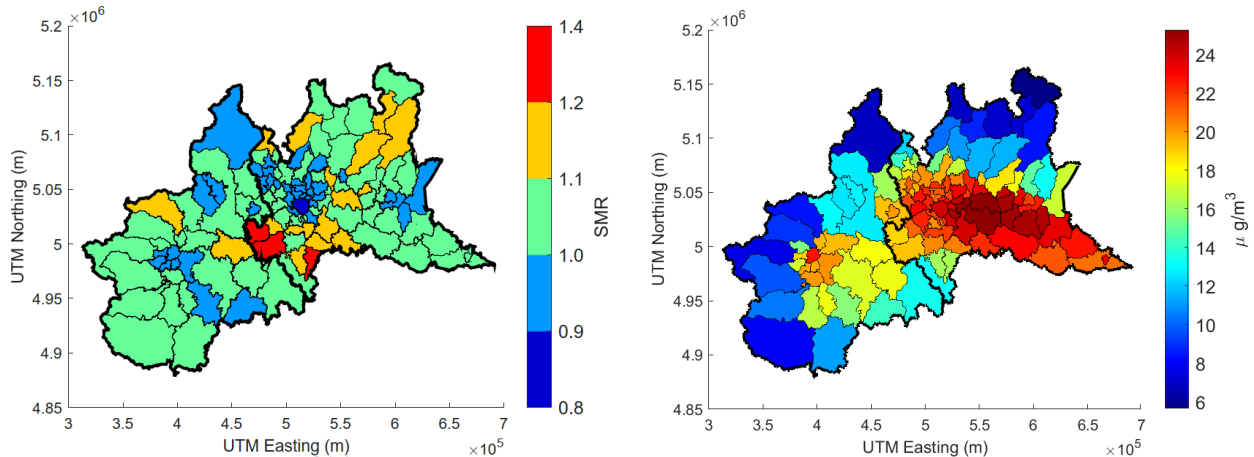


Figure 1: Long-term averages over the whole study period (2018–2022) of the SMR due to all-cause mortality (left) and of the $\text{PM}_{2.5}$ levels (right) for each HD. The thicker solid line separates Piemonte (the westernmost region) from Lombardia (the easternmost region).

2.1 Data Description

The data used in this study are retrieved from publicly available sources and full details are given in Section A of the Supplementary Material. Mortality counts are collected from the Italian National Institute of Statistics (ISTAT, 2023a), and are observed on an irregular lattice comprising $N = 117$ non-overlapping areal units termed *health districts* (HDs). The study period comprises $T = 1826$ consecutive days, hence Y_{it} denotes the number of deaths (by any cause) occurred in district $i = 1, \dots, N$ during day $t = 1, \dots, T$. The $\text{PM}_{2.5}$ concentrations are used as a measure of the exposure in district i during day t , denoted as X_{it} , and are collected from the Copernicus Atmosphere Monitoring Service’s (CAMS) Atmosphere Data Store (CAMS, 2023, INERIS et al., 2022). We also acquire information on temperature and relative humidity, which are potential confounders, from the ERA5 reanalyses dataset available at the Copernicus Climate Change Service’s (C3S) Climate Data Store (C3S, 2023, Hersbach et al., 2018). The remote-sensed measurements are spatially and temporally aggregated to match the resolution of the health data.

A measure usually employed for exploratory analyses is the standardized mortality ratio (SMR), which is calculated as $\text{SMR}_{it} = Y_{it}/E_{it}$, for $i = 1, \dots, N$ and $t = 1, \dots, T$. The denominator, E_{it} , denotes the expected number of deaths, and is computed allowing for the underlying age–sex stratification of the population within each HD (see also Section A of the Supplementary Material). Figure 1 (left panel) depicts the average daily SMR for each HD over the years 2018–2022, whose mean value is 1.25 over the whole study domain, and spatial clustering is noticeable. The right panel shows the long-term average $\text{PM}_{2.5}$ concentrations for each HD, and on average the Lombardia region is more polluted than Piemonte ($19.41 \mu\text{g}/\text{m}^3$ and $15.18 \mu\text{g}/\text{m}^3$, respectively). Other descriptive statistics are reported in Section B of the Supplementary Material.

Figure 2 shows the average daily SMR (on the logarithmic scale) for Lombardia and Piemonte. The seasonal pattern is similar in both regions, with the lowest values in summer, except for the

year 2020. Two peaks can be noticed, where the SMR more than doubled: the first one occurred in April 2020 and the other one in November 2020. These are due to the first and second “waves” of the SARS-CoV-2 pandemic, respectively. The first wave was more severe in Lombardia, while the second one was more severe in Piemonte.

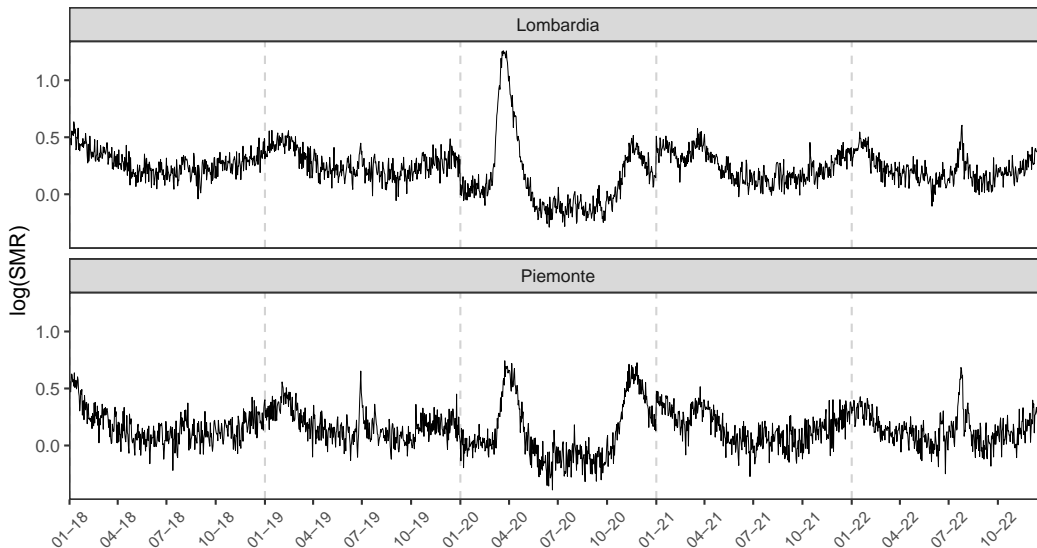


Figure 2: Time series of the average daily SMR for Piemonte (top) and Lombardia (bottom) regions, on the log scale. The vertical dashed lines separate each calendar year.

Figure 2 also highlights other two aspects. One is that the highest values of the SMR in 2018 were reached at the beginning of January, suggesting that the influenza epidemic reached its peak before the end of 2017. This is different from the year 2019, where the SMR peaks were reached in February. Another difference is that there was an increase in mortality during summer 2022. Possible reasons may be the occurrence of prolonged heat waves (indeed, the average daily temperature time-series has its absolute maximum in July 2022), or the outbreak of an influenza epidemic.

2.2 Evidence from Competing Approaches

It is assumed that the outcome follows a Poisson distribution, such that, for $i = 1, \dots, N$ and $t = 1, \dots, T$:

$$Y_{it} | \mu_{it} \stackrel{ind}{\sim} \mathcal{Poi}(\mu_{it}), \quad (1)$$

where μ_{it} indicates the mean. Then the linear predictor, $\vartheta_{it} = \ln(\mu_{it})$, is modeled as a function of exposure, X_{it} , and measured confounders, denoted as ${}^m\mathbf{Z}_{it} = ({}^mZ_{1it}, \dots, {}^mZ_{p_m it})'$, comprising basis functions of meteorological variables, and indicator variables for weekdays, national holidays, and lockdown periods (hence $p_m = 19$; see also Section A of the Supplementary Material). Additional covariates and basis functions can be included in the linear predictor to account for unmeasured confounding (see, e.g., Peng and Dominici, 2008, Peng et al., 2006). Several approaches from the

literature are then fitted under the Bayesian paradigm: (i) the Null model, which does not account for unmeasured confounding; (ii) the GLMadj model, which adjusts for unmeasured confounding through a natural cubic spline of time (see, e.g., [Masselot et al., 2022](#), [Peng and Dominici, 2008](#), [Zhou et al., 2021](#)); (iii) the JDZ model by [Janes et al. \(2007\)](#), which is similar to the previous approach but further decomposes the exposure effect in two orthogonal parts; (iv) the Dummy model (see, e.g. [Dai et al., 2014](#), [Klomp maker et al., 2023](#)), which allows for season-specific exposure effects; and (v) the Periodic model by [Peng et al. \(2005\)](#) and [Chen et al. \(2013\)](#), which assumes that the exposure effect is a linear combination of trigonometric functions. A hierarchical structure is assumed for each of them, with area-specific regression coefficients having the same mean. Further details are provided in Section C of the Supplementary Material.

Figure 3 shows, for each approach, the (overall) estimated percent change of risk associated with a $10 \mu\text{g}/\text{m}^3$ increase in $\text{PM}_{2.5}$ levels, and it can be noticed that the estimates differ considerably. The Null model yields the highest percent change on average (3.92%), whereas the JDZ model estimates the lowest percent change on average (0.47%). The models (i)–(iii) assume that the association of interest is constant over time, however this assumption is unlikely for the arguments outlined in Section 1.

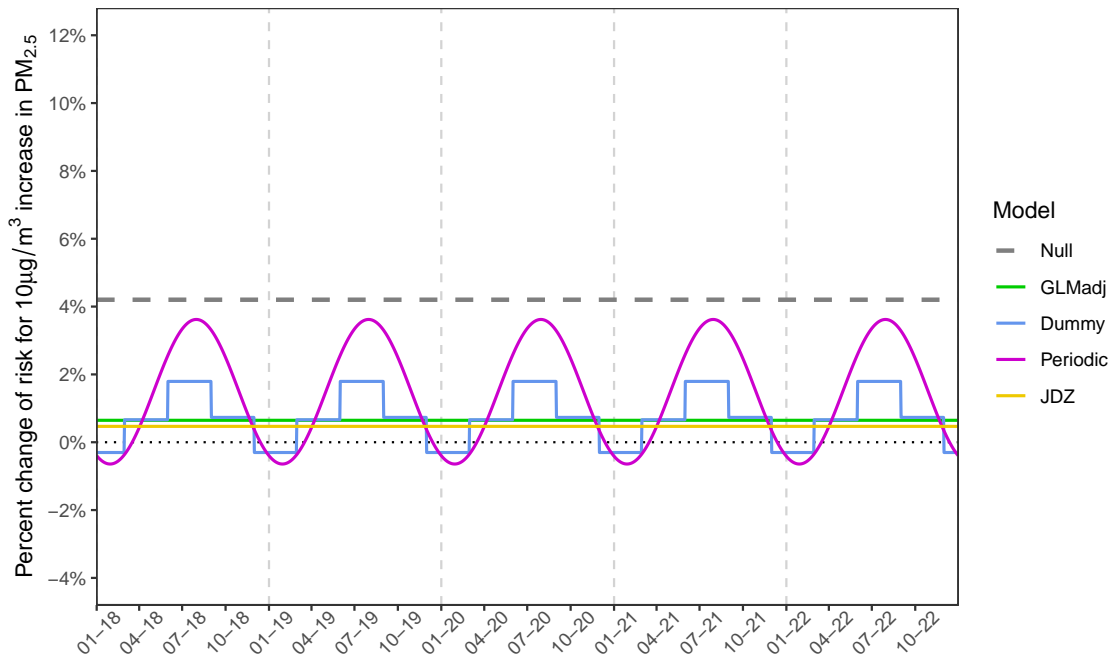


Figure 3: Estimated percent change of risk associated with a $10 \mu\text{g}/\text{m}^3$ increase in the $\text{PM}_{2.5}$ concentrations under several approaches. Null: the model that does not account for confounding; GLMadj: the model with a smooth function of time; Dummy: the model similar to GLMadj, but it also captures season-specific exposure effects; Periodic: the model similar to GLMadj where the exposure effect is assumed to be a periodic function; JDZ: the model by [Janes et al. \(2007\)](#). All models assume area-specific intercepts.

The only two approaches able to capture varying strengths of the association are the Dummy and the Periodic models. They seem to agree on the temporal evolution of the effect, showing peaks in summer and troughs in winter. Further discussion on this seemingly unexpected finding is delayed to Section 6. The Dummy and the Periodic models, however, have some limitations, since both assume that the effect changes within the year, but is the same across years. This is not consistent with the evidence from the data, as the pandemic outbreak may have altered the strength of the association. In fact, consider Figure 4, showing the average daily $PM_{2.5}$ concentrations for Lombardia and Piemonte regions. Their temporal evolutions correspond only in part to those of the SMR. In particular, the two peaks in the SMR in 2020 are not reflected in the $PM_{2.5}$ time series. Additionally, it can be noticed from Table B.3 that the overall 2020 annual mean of $PM_{2.5}$ levels was the lowest among the five years considered in our analysis. In other words, the steep increase in mortality during that year was not caused by air pollution. Instead, it is expected that people were less exposed to fine particulate matter because of the lockdown measures implemented in Italy to contain the spread of the SARS-CoV-2 virus.

Although the Dummy model allows for abrupt changes in the exposure effect, these are unlikely in practice as pointed out by [Bhaskaran et al. \(2013\)](#) and [Peng et al. \(2005\)](#). Moreover, the results may be too sensitive to the choice of the boundaries of each season, and a definition based on the calendar seasons may result suboptimal.

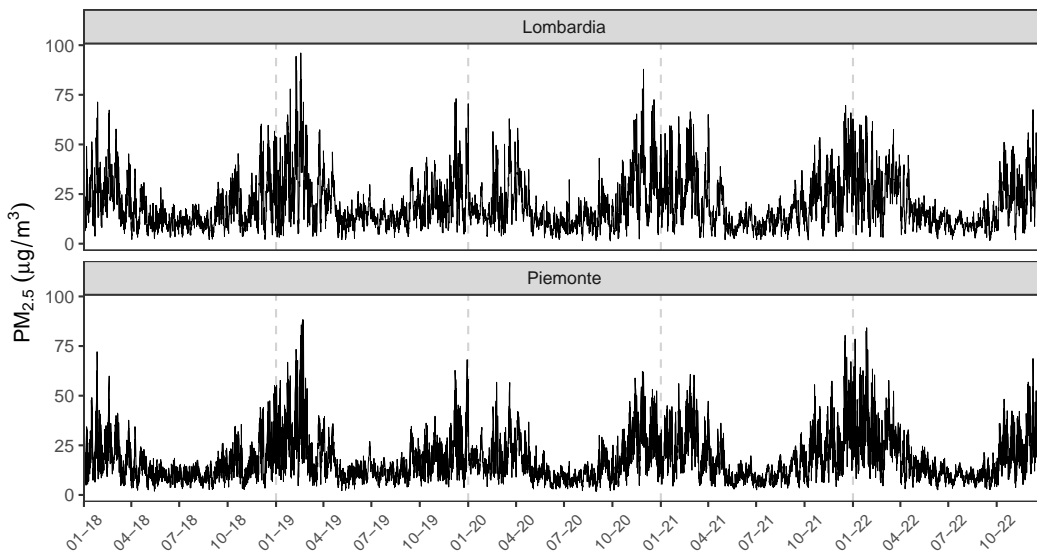


Figure 4: Time series of the average daily $PM_{2.5}$ concentrations for Piemonte and Lombardia regions. The vertical dashed lines separate each calendar year.

3 The Proposed Model

For $i = 1, \dots, N$ and $t = 1, \dots, T$, let Z_{it} denote an unmeasured confounder. We assume that ${}^m\mathbf{Z}_{it}$ and Z_{it} are spatially and temporally smoother than the exposure, and that the outcome follows the distribution in Equation (1). The linear predictor is then specified as:

$$\vartheta_{it} = o_{it} + \beta_{0i} + f(X_{it}; \gamma_f) + {}^m\mathbf{Z}'_{it}\boldsymbol{\alpha}_m + Z_{it} + u_{it}, \quad (2)$$

where o_{it} is the offset, β_{0i} is an area-specific intercept, $f(\cdot; \cdot)$ is an unknown smooth function parameterized by the vector γ_f , $\boldsymbol{\alpha}_m$ is a p_m -dimensional vector of coefficients, and u_{it} is a spatially and temporally uncorrelated Gaussian random variable, assumed to have zero mean and constant variance, i.e. $u_{it} \stackrel{iid}{\sim} \mathcal{N}(0, \tau_u^2)$.

If all confounders were measured and $f(\cdot; \cdot)$ was modeled using basis functions, the model specification in Equations (1)–(2) would belong to the family of generalized additive models (GAMs; see [Wood, 2017](#)). Alternatively, considering that $f(\cdot; \cdot)$ can be adequately approximated by using the first-order Taylor’s expansion, we have:

$$f(X_{it}; \gamma_f) = f(\widehat{X}_t; \gamma_f) + f'(\widehat{X}_t; \gamma_f)(X_{it} - \widehat{X}_t) + \varpi_{it}, \quad (3)$$

where \widehat{X}_t denotes the large-scale (or *overall*) temporal trend, $f'(\widehat{X}_t; \gamma_f)$ is the first derivative of $f(\cdot; \gamma_f)$ with respect to its first argument, evaluated at \widehat{X}_t , and ϖ_{it} denotes the Taylor’s remainder. The overall temporal trend can be calculated as a spatial average at each $t = 1, \dots, T$. Alternatively, X_{it} can be regressed on a smooth function of time (see also [Janes et al., 2007](#)):

$$X_{it} = h(t; df) + \nu_{it}, \quad (4)$$

where df are the degrees of freedom of the smooth term, and ν_{it} is an uncorrelated Gaussian random variable with zero mean and constant variance. The overall temporal trend is then defined as the fitted values obtained from the model (4), i.e. $\widehat{X}_t = \widehat{h}(t; df)$.

Equation (3) provides a decomposition of the exposure effect into two components describing large and small (or *local*) scales of variation. These components are functions of \widehat{X}_t and $X_{it} - \widehat{X}_t$, respectively. They are orthogonal because $X_{it} - \widehat{X}_t$ is the residual term from the regression in Equation (4). Henceforth, the decomposition above should help to disentangle the effect of interest from that of unmeasured confounding factors. To clarify this, consider that \widehat{X}_t captures trend and seasonal components of the exposure, therefore it is expected to be highly correlated with Z_{it} , given that the latter is smooth, while the correlation between $X_{it} - \widehat{X}_t$ and Z_{it} should be close to zero. Therefore, the unmeasured confounder is more likely to affect the association between outcome and exposure at large scales ([Greven et al., 2011](#), [Janes et al., 2007](#)), so the first term in the decomposition of $f(X_{it}; \gamma_f)$ in Equation (3) might be biased, but it is less likely that the second term, $f'(\widehat{X}_t; \gamma_f)(X_{it} - \widehat{X}_t)$, is affected by confounding bias.

By decomposing $f(X_{it}; \gamma_f)$ in Equation (2), we thus have:

$$\vartheta_{it} = o_{it} + \beta_{0i} + f(\widehat{X}_t; \gamma_f) + f'(\widehat{X}_t; \gamma_f)(X_{it} - \widehat{X}_t) + {}^m \mathbf{Z}'_{it} \boldsymbol{\alpha}_m + Z_{it} + \tilde{u}_{it}. \quad (5)$$

where $\tilde{u}_{it} = u_{it} + \varpi_{it}$ is such that $\tilde{u}_{it} \stackrel{iid}{\sim} \mathcal{N}(0, \tilde{\tau}_u^2)$.

The unknown function evaluated at the overall temporal trend of the exposure, $f(\widehat{X}_t; \gamma_f)$, and its first derivative in Equation (5) can be seen as functions of time, therefore a time-varying coefficients can adequately represent them (see also West and Harrison, 1997, Section 3.1). Therefore, we propose to change the linear predictor in Equation (2) for:

$$\vartheta_{it} = o_{it} + \beta_{0it} + \beta_{1t}(X_{it} - \widehat{X}_t) + {}^m \mathbf{Z}'_{it} \boldsymbol{\alpha}_m + \tilde{u}_{it}, \quad (6)$$

where $\beta_{1t} = f'(\widehat{X}_t; \gamma_f)$ is the time-varying coefficient representing the local association between exposure and outcome (in the sense of Janes et al. (2007)), while β_{0it} is a time-varying area-specific intercept,

$$\beta_{0it} = \beta_{0i} + f(\widehat{X}_t; \gamma_f) + Z_{it},$$

that should account for both the large-scale exposure effect and the unmeasured confounder.

We now provide two examples of the function $f(\cdot; \cdot)$ and of the resulting time-varying coefficients in Equation (6). These show that our model generalizes other methods in the literature.

Example 3.1. If $f(\cdot; \gamma_f)$ is a constant function, i.e. $f(X_{it}; \gamma_f) = \gamma_{f0}$, then $\beta_{1t} = 0$ and $\beta_{0it} = \beta_{0i} + \gamma_{f0} + Z_{it}$.

Example 3.2. If $f(\cdot; \gamma_f)$ is a linear function, i.e. $f(X_{it}; \gamma_f) = \gamma_{f0} + \gamma_{f1} X_{it}$, then $\beta_{1t} = \gamma_{f1}$ and $\beta_{0it} = \beta_{0i} + \gamma_{f0} + \gamma_{f1} \widehat{X}_t + Z_{it}$. The model proposed by Janes et al. (2007) can be cast in this case, with $\gamma_{f0} = 0$. The authors, however, assume further that the intercepts are constant, so the overall trend in the exposure is included as a covariate. They also include a smooth function of time in their specification to control for seasonality and long-term trends common to all areas.

3.1 Specification of the Time-Varying Coefficients

We implement a DGLM with random walk processes to model the temporal evolution of the regression coefficients β_{0it} and β_{1t} . We propose the following state-space formulation for the latent process and the regression coefficients, for $t = 1, \dots, T$:

$$\boldsymbol{\vartheta}_t = \mathbf{o}_t + \tilde{\mathbf{X}}_t \tilde{\boldsymbol{\beta}}_t + {}^m \mathbf{Z}_t \boldsymbol{\alpha}_m + \tilde{\mathbf{u}}_t, \quad \tilde{\mathbf{u}}_t \sim \mathcal{N}(\mathbf{0}, \tilde{\tau}_u^2 \mathbf{I}_N) \quad (7)$$

$$\tilde{\boldsymbol{\beta}}_t = \tilde{\boldsymbol{\beta}}_{t-1} + \mathbf{w}_t, \quad \mathbf{w}_t \sim \mathcal{N}(\mathbf{0}, \boldsymbol{\Sigma}_w), \quad (8)$$

where $\boldsymbol{\vartheta}_t = (\vartheta_{1t}, \dots, \vartheta_{Nt})'$, $\mathbf{o}_t = (o_{1t}, \dots, o_{Nt})'$,

$${}^m\mathbf{Z}_t = \begin{bmatrix} {}^m\mathbf{Z}'_{1t} \\ \vdots \\ {}^m\mathbf{Z}'_{Nt} \end{bmatrix},$$

and $\tilde{\boldsymbol{\beta}}_t = (\beta_{01t}, \dots, \beta_{0Nt}, \beta_{1t})'$ is an $(N + 1)$ -dimensional vector. The observation matrix is $\tilde{\mathbf{X}}_t = \begin{bmatrix} \mathbf{I}_N & \tilde{\mathbf{X}}_{\cdot t} \end{bmatrix}$, where

$$\tilde{\mathbf{X}}_{\cdot t} = \begin{bmatrix} X_{1t} - \widehat{X}_t \\ \vdots \\ X_{Nt} - \widehat{X}_t \end{bmatrix}.$$

4 Bayesian Inference and Computations

The first stages of the Bayesian hierarchical model are defined by Equations (1) and (7)–(8). To complete it, a prior distribution must be assigned on the parameter set, $\Theta = \{\tilde{\boldsymbol{\beta}}_0, \boldsymbol{\alpha}_m, \boldsymbol{\Sigma}_w, \tilde{\tau}_u^2\}$.

4.1 Prior Specification

Independent prior distributions are imposed on each parameter in Θ . As for the vector of time-varying coefficients, $\tilde{\boldsymbol{\beta}}_t$, distributional assumptions are required on the initial state (i.e., when $t = 0$), and on the innovation error covariance matrix, $\boldsymbol{\Sigma}_w$. We impose that $\tilde{\boldsymbol{\beta}}_0 \sim \mathcal{N}(\mathbf{0}, \mathbf{V}_\beta)$, where

$$\mathbf{V}_\beta = \begin{bmatrix} 10\mathbf{I}_N & \mathbf{0} \\ \mathbf{0} & 4 \times 10^{-6} \end{bmatrix}.$$

The prior specification for $\boldsymbol{\Sigma}_w$ requires more care. We assume that this matrix is block-diagonal, i.e. $\boldsymbol{\Sigma}_w = \begin{bmatrix} \boldsymbol{\Sigma}_{w0} & \mathbf{0} \\ \mathbf{0} & \sigma_{w1}^2 \end{bmatrix}$. Given that the area-specific intercepts should capture the effect of the unmeasured confounder, Z_{it} , we expect them to be spatially correlated, so $\boldsymbol{\Sigma}_{w0}$ is an $N \times N$ matrix for which an inverse-Wishart prior is assigned, i.e. $\boldsymbol{\Sigma}_{w0} \sim \mathcal{IW}(a_{w0}, \mathbf{S}_{w0})$, with $a_{w0} = N + 2$ and $\mathbf{S}_{w0} = k_0\mathbf{I}_N$. This specification allows for a free-form and data-driven covariance structure, and facilitates inference, since the posterior full conditional distribution of $\boldsymbol{\Sigma}_{w0}$ is available in closed-form (Brown et al., 1994). An inverse-gamma prior is imposed on σ_{w1}^2 , i.e. $\sigma_{w1}^2 \sim \mathcal{IG}(a_{w1}, b_{w1})$. Other specifications were also considered (e.g., $\boldsymbol{\Sigma}_w$ was assumed to be diagonal), but they did not provide good mixing of the posterior samples chains. Recall that capturing gradual changes is a desired feature of the proposed model, and the matrix $\boldsymbol{\Sigma}_w$ plays a crucial role to this end. For instance, if k_0 is “large”, the short-term variation in the intercepts becomes unlikely pronounced, whereas if k_0 is “small”, the “true” variation is captured only in part. The definition of “large” and “small” mainly depends on the sample size and on how much the prior dominates the likelihood. Note also that extreme values of k_0 may lead to numerical non-positive definiteness of $\boldsymbol{\Sigma}_{w0}$.

Therefore, several values for the hyperparameters k_0 , a_{w1} and b_{w1} are considered to evaluate the sensitivity of the posterior distribution to the prior. In the case of both simulated and real data (see Sections 5 and 6, respectively), we find that $k_0 = 10^{-3}$, $a_{w1} = 11$, and $b_{w1} = 10^{-6}$ provide a good balance between the prior and the likelihood.

Finally, non-informative normal priors are imposed on the coefficients of the measured confounders, $\boldsymbol{\alpha}_m \sim \mathcal{N}(\mathbf{0}, 10^6 \mathbf{I}_{p_m})$. Following Wakefield (2007), it is assumed that the residual relative risks \tilde{u}_{it} , follow a log- t distribution with two degrees of freedom, and with 95% of prior mass within the interval (0.98, 1.02), hence we obtain the prior $\tilde{\tau}_u^2 \sim \mathcal{IG}(1, 2.1 \times 10^{-5})$.

4.2 Computations

As first step of the analysis, the overall temporal trend, \widehat{X}_t , is obtained as the fitted values from the model in Equation (4), where $h(t; df)$ represents a natural cubic spline of time with df degrees of freedom. This two-step strategy should be preferred to a joint modeling of the exposure and the outcome, as it allows avoiding feedback from the outcome to the exposure that may lead to biased estimators of the exposure effect (see, e.g., Stephens et al., 2023).

An MCMC scheme is then implemented to simulate from the posterior distribution of Θ . The algorithm proposed by Chan and Jeliaskov (2009) is used to sample from the full conditionals of the time-varying coefficients. It is an efficient simulation algorithm that allows to sample all the regression coefficients (for all the time instants) in a single step. The remaining full conditional distributions are composed of inverse-gamma, and inverse-Wishart distributions. The latent process ϑ_{it} is an exception and is sampled using a Metropolis-Hastings step. Further details can be found in Section D of the Supplementary Material.

5 Analysis of Artificial Data

To validate the proposed approach, we conduct two simulation studies, both inspired by the real data example presented in Section 2. In the first one, which is described next, we want to assess the ability of the proposed model to mitigate the confounding bias.

Simulation Study 1: Confounding Bias Mitigation We consider $N = 100$ contiguous HDs of Piemonte and Lombardia, then we assume that $T = 300$, that there are no measured confounders (i.e., $p_m = 0$) and that the exposure X_{it} and the unmeasured confounder Z_{it} are correlated vector autoregressive processes of order 1 (VAR(1)) with a linear correlation coefficient $\rho_{xz} = \text{Cor}(X_{it}, Z_{it}) = 0.5$, for $i = 1, \dots, N$, and $t = 1, \dots, T$, and with spatially-structured, temporally independent innovations (Cressie and Wikle, 2015, Sahu, 2022). A proper conditional autoregressive (PCAR) specification (Banerjee et al., 2014, Besag, 1974, Sahu, 2022) is assumed to model the spatial dependence of these innovations. The marginal spatio-temporal means of expo-

sure and unmeasured confounder are generated from Fourier basis expansions with period T . The correlation matrix of X_{it} is parameterized by spatial and temporal autocorrelation parameters, i.e. $\phi_x^S \in (0, 1)$ and $\phi_x^T \in (0, 1)$, respectively. Similarly, ϕ_z^S and ϕ_z^T represent the autocorrelation parameters of Z_{it} , which is sampled conditional on X_{it} . These four parameters represent the strength of the spatial and temporal dependence, and define three scenarios that are summarized in Table 1. The outcome variable is sampled from the Poisson distribution in Equation (1) using the following linear predictor:

$$\vartheta_{it} = o_{it} + \beta_{0i} + \beta_{1t}X_{it} + Z_{it} + u_{it}, \quad u_{it} \stackrel{iid}{\sim} \mathcal{N}(0, \tau_u^2),$$

where $\tau_u^2 = 10^{-5}$. Additional information on the data generation mechanism is provided in Section E of the Supplementary Material.

Table 1: Simulation scenarios and corresponding definitions.

Scenario	Unmeasured confounder, Z_{it}	ϕ_x^S	ϕ_z^S	ϕ_x^T	ϕ_z^T
S1	Smoother than exposure in space and time	0.2	0.98	0.2	0.98
S2	Smoother than exposure only in space	0.2	0.98	0.98	0.2
S3	Smoother than exposure only in time	0.98	0.2	0.2	0.98

The proposed approach is compared to the Null model and to the GLMadj model, where natural cubic spline of time with 7 degrees of freedom is used for the latter. Following Peng et al. (2006), the degrees of freedom for the spline are chosen by fitting several models with different numbers of bases and selecting the minimum number from which the estimates appear stabilized.

Figure 5 depicts the results in terms of percent change of risk associated with a 10-unit increase in the exposure, defined as $P_t = 100(\exp\{10\beta_{1t}\} - 1)$. For each scenario, the black solid line represents the case where true exposure effect is a constant (top), a periodic (middle), or a more complex function of time (bottom). The estimate of P_t obtained from the proposed DGLM is shown in red, with the solid line indicating its average, and the shaded area indicating the percentiles 2.5 and 97.5 of its distribution over 100 replicates.

The dashed gray and dashed green lines represent the estimated percent changes of risk from the Null and GLMadj models, averaged over the 100 replicates. Whereas the Null model is evidently biased in all cases, the GLMadj model and the proposed approach significantly reduce the confounding bias in Scenario S1, although without entirely removing it. In Scenario S2, the confounding bias reduction is still achieved by the DGLM compared to the Null model, but to a lesser extent. This could be because the unmeasured confounder varies at high frequencies in time, so it cannot be captured by the time-varying intercepts that only account for gradual changes. Also, the difference $X_{it} - \widehat{X}_t$ is approximately as rough as Z_{it} , and, due to their correlation, a portion of the variability of the unmeasured confounder is explained by the local exposure effect. Scenario S3 is very similar to Scenario S1, suggesting that the lack of smoothness in space of the unmeasured confounder does not seem to alter the performance (in terms of confounding bias) of the proposed approach.

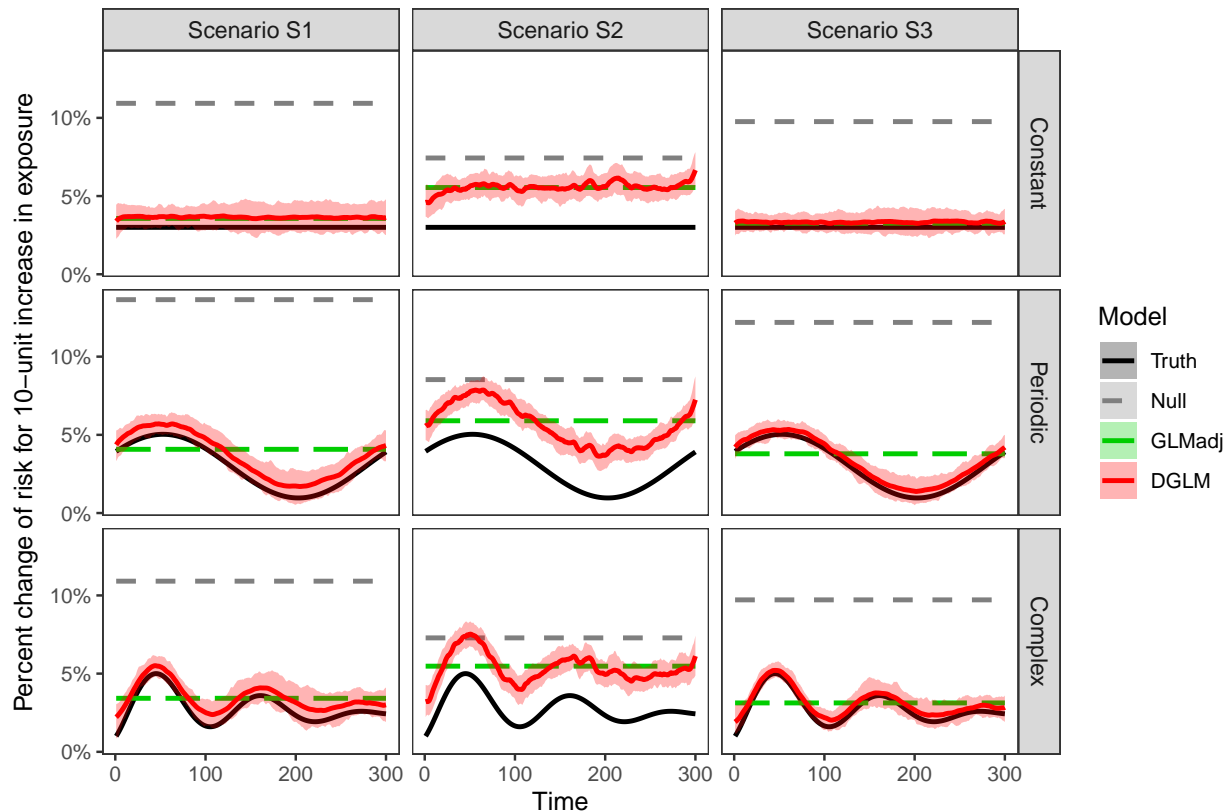


Figure 5: Simulation Study 1: results are expressed in terms of percent change of risk associated with a 10-unit increase in the exposure, P_t . The black solid line represents the true exposure effect (whose shape differs in each row), while the dashed gray line represents the estimated exposure effect from the Null model. The red solid line and the shaded area represent the average and the percentiles 2.5 and 97.5 of the posterior means of P_t obtained from the proposed DGLM over 100 replicated datasets.

These results are confirmed also by Table E.4 in the Supplementary Material, where the average mean squared error (MSE_{avg}), the maximum absolute bias (MAB), and the average mean absolute error (MAE_{avg}) are reported for each model and each scenario (see the Supplementary Material, Section E.2, for definitions). The GLMadj model has the lowest values when the exposure effect is constant. This is likely because the GLMadj model correctly assumes a constant exposure–outcome relationship, whereas the proposed model learns its shape from the data. Nevertheless, in the top subplots of Figure 5, horizontal straight lines can be drawn through the red shaded areas, indicating that the DGLM correctly identifies a constant exposure effect. In the remaining cases, the proposed model seems to perform best, as it is able to capture the temporal variations of the true exposure effect.

Model Reparameterization Section E.3 of the Supplementary Material also motivates, from a practical viewpoint, the decomposition of the exposure effect into the two components described

in Equation (3). We compare the proposed DGLM with a reparameterized model that does not remove the overall trend from the exposure. The results suggest that the proposed approach is more effective in reducing the confounding bias and almost always has lower MSE_{avg} , MAB and MAE_{avg} values.

Simulation Study 2: Recovery of the Local Exposure Effect (f') In the second simulation study, described in Section F of the Supplementary Material, we want to assess whether the proposed DGLM is able to recover $f'(\cdot; \gamma_f)$, i.e. the first derivative of the unknown functional form. The data are generated using Equations (1)–(2), and we show that the DGLM is able to capture the dynamics of the exposure effect, but there remains a residual bias which is only due to confounding (i.e., not due to Taylor’s approximation).

6 Application to the Italian Mortality Data

We now apply the proposed DGLM to the Italian mortality dataset (see Section 3). The overall trend, \widehat{X}_t , is obtained using a natural cubic spline of time with 4 degrees of freedom per year. For each HD and time instant, ${}^m\mathbf{Z}_{it}$ contains bases from a natural cubic spline of daily temperature and daily relative humidity (with 7 and 4 degrees of freedom, respectively), indicator variables for weekdays, for holidays, and for the lockdown periods.

The MCMC algorithm described in Section 4 is run for 100,000 iterations, and posterior inference is based on the final 80,000 draws. The model’s chains are monitored for convergence visually through trace plots and using the R-statistic of Gelman (1996) on two chains that are started from different initial points simultaneously.

We assess the adequacy of the model fit by analyzing Bayesian p -values for each HD and time instant. The chosen measure evaluates how well the model aligns with the observed data, and involves calculating the quantity $\Pr(Y_{it} > Y_{it}^{rep}) + \frac{1}{2} \Pr(Y_{it} = Y_{it}^{rep})$, where Y_{it}^{rep} is generated from the predictive distribution in each MCMC iteration. Bayesian p -values close to 0.5 suggest that the generated data align well with the model. Conversely, values approaching the boundaries of the unit interval, i.e. < 0.1 or > 0.9 , indicate a poor fit (Gelman et al., 2013). The estimated mean p -value is around 0.5 suggesting an adequate fit.

Figure 6 depicts the estimated local exposure effect, expressed in terms of percent change of risk associated with a $10 \mu\text{g}/\text{m}^3$ increase in the $\text{PM}_{2.5}$ concentrations. The red solid line represents its posterior mean, while the shaded area the corresponding 95% credible interval (CI). The exposure effect is not constant in time, as no horizontal straight line can be drawn within the CI. This effect, instead, exhibits varying peaks across different years, and three phases are clearly identifiable: before (2018-19), during (2020-21) and after (2022) the pandemic outbreak.

During the first two years, the local exposure effect exhibits a seasonal pattern, with the peaks occurring during the summer months. The estimated association is bounded away from zero from

July to October 2018 from April to September 2019, with the highest change in mortality risk of 7.47% (95% CI: [3.88%, 11.30%]) occurring on June 29, 2019.

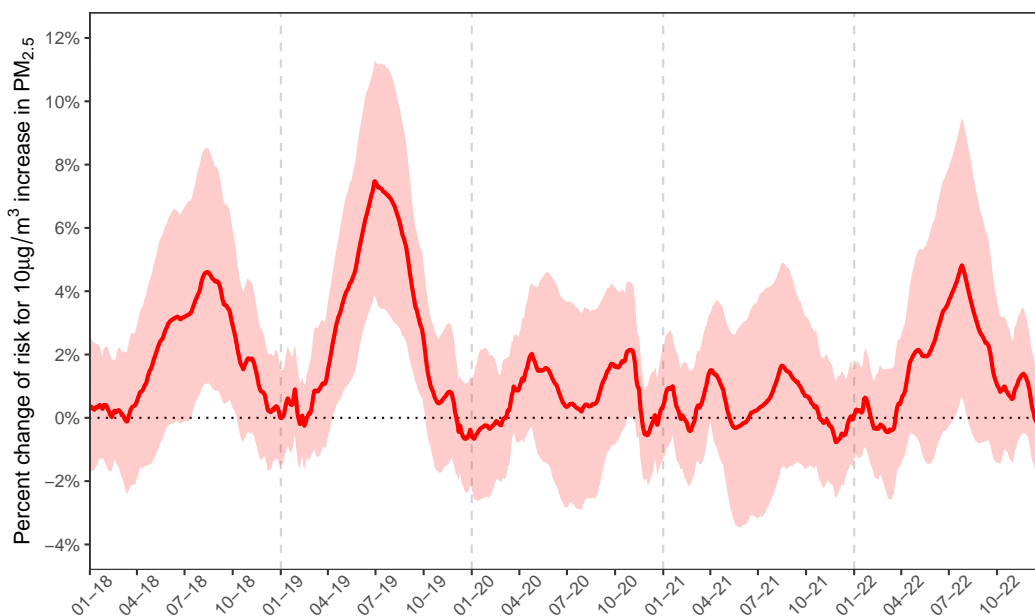


Figure 6: Time-varying percent change of risk associated with a $10 \mu\text{g}/\text{m}^3$ increase in the $\text{PM}_{2.5}$ concentrations estimated by the proposed DGLM. The red solid line represents its posterior mean, while the shaded area the corresponding 95% CI.

It is worth noting that a higher percent change of mortality risk occurs when the fine particulate matter is generally less present in the air, so this may indicate that a threshold below which the exposure effect is null might not exist (see, among others, [Brunekreef et al., 2021b](#), [Cork et al., 2023](#), [Dominici et al., 2022](#), [Renzi et al., 2021](#)). The seasonal behavior seems to be confirmed by other studies ([Nawrot et al., 2007](#), [Peng et al., 2006](#), [Roberts, 2004](#), [Stafoggia et al., 2008](#), [Sun et al., 2015](#), [Tian et al., 2018](#)).

These seasonal changes of the risk might be due to potential interaction effects of $\text{PM}_{2.5}$ concentrations with air temperature. As noted in Section 1, increased ventilation and physiological susceptibility to air pollution may explain the higher percent change of risk during summer. Of course, interaction with other variables, such as other pollutants, are also possible (see, e.g., [Ji et al., 2022](#), [Liu et al., 2023](#), [Siddika et al., 2019](#)).

Previous studies have also reported that particle composition may modify the effect of $\text{PM}_{2.5}$ on mortality. In fact, fine particulate matter is a complex mixture of organic (such as black carbon and organic carbon) and inorganic compounds (such as sulfate, nitrate, and ammonium), and the relative proportion of these components may vary in time ([Franklin et al., 2008](#), [Massetot et al., 2022](#), [Vinson et al., 2020](#)). Indeed, their precursors are emitted from both natural (e.g., oceans and volcanoes) and anthropogenic sources, such as fossil fuel combustion, industrial processes, and residential heating, and their transportation and transformation to $\text{PM}_{2.5}$ in the atmosphere are

mainly influenced by meteorological conditions (Hao et al., 2023, Jing et al., 2020, Kelly and Fussell, 2012). Toxicological studies indicate that the PM constituents have different effects on human health (see, e.g., Kelly and Fussell, 2012), and some authors have suggested that ammonium is probably among the most harmful components (Hao et al., 2023, Masselot et al., 2022).

During the pandemic phase, the CI always contains the zero except for few days in October 2020. The literature reveals a lack of consensus regarding the association between air pollution and adverse COVID-19 health outcomes in the general population (see, for example, Brunekreef et al., 2021a, Walton et al., 2021). More recently, the review by Bhaskar et al. (2023) suggests a positive association in the majority of previous studies. Our findings, instead, indicate that the local exposure effect in 2020 and 2021 is generally not bounded away from zero. To justify this, consider first of all that our model uses all-cause mortality in the elderly population as the health outcome, so it is not directly comparable to the COVID-19 studies mentioned earlier. Secondly, the issuance of the lockdown measures by the Italian government, as well as the mandatory use of facial masks, not only effectively curbed the transmission of the SARS-CoV-2 virus (and of other viruses), but also potentially reduced exposure to air pollution. During the lockdown periods, people were required to stay at home, resulting in reduced exposure to outdoor air pollutants. The ventilation was limited because the lockdowns occurred during non-summer months. Moreover, the use of facial masks may have reduced the inhalation of airborne hazardous particles (Kodros et al., 2021, Zhou et al., 2018).

Although lockdown periods were not issued in the second half of 2021, the local exposure effect remains not bounded away from zero. This could be due to the fact that people continued to adopt measures such as wearing masks and sanitizing hands. Additionally, it is possible that the phenomenon of *mortality displacement* or *harvesting* may have occurred. This is a consequence of the fact that the most vulnerable people may have died earlier than expected in the preceding years due to the SARS-CoV-2 virus in 2020-2021, resulting in an apparently null (or even protective) effect of the exposure afterwards (Armstrong et al., 2017, Bhaskaran et al., 2013, Zanobetti and Schwartz, 2008, Zanobetti et al., 2000).

In the third phase, people started to return to their normal activities, resulting in increased exposure to air pollution. In fact, the local exposure effect has a shape similar to that in 2018, but is bounded away from zero only in July 2022 (probably because of mortality displacement), with the highest change in mortality risk of 4.82% (95% CI: [0.65%, 9.46%]) occurring on July 26.

Comparison with a Restricted Model In Section G of the Supplementary Material we want to understand the consequences of removing the measured confounders (i.e., temperature, relative humidity, and indicators for weekdays, national holidays, and lockdown periods) from the model specification. Therefore, we impose the restriction that the elements of α_m in Equation (6) are zero. The results are insightful, as the estimated exposure effect greatly overlaps the estimate obtained when the measured confounders are included, with differences occurring only in summer.

This suggests that the proposed DGLM can provide accurate estimates even in complex scenarios, and that the confounding effect may be time-varying and may be due to heat waves.

7 Discussion

Motivated by a real case-study, in this paper we have proposed a DGLM as a solution for two types of bias that may affect the estimation and interpretation of the exposure–outcome relationship: misspecification and confounding bias. Misspecification bias arises from assuming that the exposure effect is constant in time when it is not. When analyzing the health effects of air pollution, [Chiogna and Gaetan \(2002\)](#) and [Peng et al. \(2005\)](#), among others, argue that there is uncertainty about the “true” functional form of the exposure–outcome association. Therefore, assuming a constant effect may be too restrictive and result in biased estimates. We acknowledge this fact and assume that there exists a smooth (but unknown) function of the exposure, $f(\cdot; \cdot)$, describing the association of interest. Confounding bias is due to the presence of an unmeasured confounder. To control for it, we decompose the exposure effect into large- and small-scale components following [Janes et al. \(2007\)](#), but, differently from them, we assume that the local effect is time-varying.

We have shown that the proposed approach enjoys some advantages. On one hand, it is able to capture any time-varying exposure effect, thus overcoming the misspecification bias. On the other hand, thanks to the first-order Taylor’s expansion, the DGLM can model the local exposure effect within a flexible framework, thus mitigating the confounding bias. In this sense, the proposed approach constitutes an extension of the model suggested by [Janes et al. \(2007\)](#).

The effectiveness of the proposed approach has been demonstrated through artificial data analyses. We have shown that it performs better than the Null and the GLMadj models. In particular, the proposed DGLM not only can reduce the bias, but also can capture complex temporal fluctuations of the exposure effect and almost recover its true functional form. The bias is less alleviated when the unmeasured variable is less smooth than the exposure in time, but it is worth noticing that this situation is rather unrealistic in practice. We have seen that the GLMadj model could achieve the lowest average mean squared error in the case of a constant exposure effect (see Table E.4), however, the shape of the exposure–outcome association is typically unknown. Unless there is strong prior information about this shape, we thus suggest using the proposed DGLM. Furthermore, as a proof of concept, in Section F of the Supplementary Material, we set up a scenario where a complete absence of confounders is assumed. In this case, the exposure effect results fully recovered.

Many previous empirical works assume an exposure–outcome association constant in time. However, the evidence from the analysis of the Italian mortality data have indicated that this assumption is conceivably incorrect. In fact, the estimated local exposure effect exhibits a seasonal pattern, with a higher percent change of risk observed during the summer months, when the overall PM_{2.5} level is lower. Similar conclusions were reached in other studies ([Peng et al., 2005, 2006](#), [Roberts, 2004](#), [Stafoggia et al., 2008](#), [Sun et al., 2015](#), [Tian et al., 2018](#)). Although this fact is apparently

counterintuitive, it has been observed that it might be due to possible interaction effects of $\text{PM}_{2.5}$ concentrations with meteorological variables, such as temperature, and other air pollutants. We have also noted that our result may be related to possible effect modification due to changes in the particulate matter mixture (Franklin et al., 2008, Hao et al., 2023, Masselot et al., 2022). The relative proportions of the $\text{PM}_{2.5}$ components have not been analyzed in this study, so they could be the subject of future research. However, it is important to note that Hao et al. (2023) found a non-linear long-term association between some $\text{PM}_{2.5}$ constituents and mortality.

An exception to the seasonal behavior are the years 2020 and 2021, when the exposure effect is not bounded away from zero. This can be justified by the fact that the lockdown measures, such as stay-at-home orders and the use of masks, have likely reduced the exposure to air pollution. It is worth recalling that none of the competing approaches in Section 2 were able to capture this behavior. Additionally, our findings may contradict the results of the majority of studies reviewed in Bhaskar et al. (2023). However, there are differences in the definition of outcomes between our analysis and theirs, as we focused on all-cause mortality in the elderly population. Moreover, not all studies related to COVID-19 properly account for potential confounders, so their findings should be interpreted with caution (Bhaskar et al., 2023, Brunekreef et al., 2021b, Walton et al., 2021). In contrast, the proposed DGLM is able to almost completely capture the exposure effect even in the absence of measured confounders (see Figure G.5 in the Supplementary Material).

To account for the residual spatial autocorrelation in the outcome, possibly due to unmeasured confounding, the proposed model can potentially provide for the adjacency of areal units, a feature often ignored in *multi-site time-series studies* (see, e.g., Dai et al., 2014, Janes et al., 2007, Peng et al., 2005, Qiu et al., 2022, Zhou et al., 2021). In fact, this could be achieved by including into the linear predictor a spatially structured random effect with a conditional autoregressive specification. On the other hand, our model cannot consider spatial variations of the local exposure effect, so it would be interesting to specify a spatially-varying coefficients model, which would allow discovering differences due to urbanicity and morphology of the study area, for example.

The decomposition of the exposure effect into two orthogonal components allows Janes et al. (2007) to test for the presence of unmeasured confounders. The authors state that if the overall and local exposure effects are equal, then it is likely that the confounding bias is not present. In our case, this testing procedure is theoretically possible, but it is not straightforward to implement in practice, since specific assumptions on the functional form of $f(\cdot; \gamma_f)$ are required.

It is arguable that, even if the proposed DGLM could recover the true exposure effect, $f(\cdot; \cdot)$, its functional form still remains unknown. In other words, the complete list of interaction terms cannot be determined. However, we believe that this is not a drawback only of the proposed model. In fact, the list of interaction terms is unknown when fitting any regression model, and it is up to the researcher to choose the most appropriate form for $f(\cdot; \cdot)$. This decision may involve some degree of uncertainty. The proposed approach, instead, allows for more flexibility and should be able to capture the effect of lockdowns as well as interaction effects between the exposure and

other variables, such as other pollutants, so that inferential problems due to misspecification are overcome.

In conclusion, the proposed DGLM is a flexible and effective approach to estimate the exposure–outcome association in the presence of time-varying effects and unmeasured spatio-temporal confounding. The model is able to capture the complex dynamics of the exposure effect, and to control for confounding. Also, in the scenario simulated without confounding, the true effect is correctly recovered. The proposed approach is a valuable tool for researchers interested in the health effects of air pollution, and it can be extended to other fields where the exposure–outcome association is of interest.

Acknowledgements

Hersbach et al. (2018) was downloaded from the C3S (2023). INERIS et al. (2022) was downloaded from the CAMS (2023). The results contain modified C3S and CAMS information. Neither the European Commission nor ECMWF is responsible for any use that may be made of the Copernicus information or data it contains. The research of Zaccardi, Valentini and Ippoliti is funded by the European Union - NextGenerationEU, research project PRIN2022 CoEnv - Complex Environmental Data and Modeling (CUP 2022E3RY23). Schmidt is grateful for financial support from the Natural Sciences and Engineering Research Council (NSERC) of Canada (Discovery Grant RGPIN-2017-04999).

Bibliography

- A. Adin, T. Goicoa, J. S. Hodges, P. M. Schnell, and M. D. Ugarte. Alleviating confounding in spatio-temporal areal models with an application on crimes against women in india. *Statistical Modelling*, 23(1):9–30, 2023.
- O. A. Alduchov and R. E. Eskridge. Improved magnus form approximation of saturation vapor pressure. *Journal of Applied Meteorology and Climatology*, 35(4):601–609, 1996.
- A. Analitis, K. Katsouyanni, X. Pedeli, U. Kirchmayer, P. Michelozzi, and B. Menne. Investigating the independent and synergistic effects of heat waves and air pollution on health: The euroheat project. *Epidemiology*, 19(1):S214–S215, 2008.
- A. Analitis, P. Michelozzi, D. D’Ippoliti, F. De’Donato, B. Menne, F. Matthies, R. W. Atkinson, C. Iñiguez, X. Basagaña, A. Schneider, et al. Effects of heat waves on mortality: effect modification and confounding by air pollutants. *Epidemiology*, pages 15–22, 2014.
- A. Analitis, F. De’Donato, M. Scortichini, T. Lanki, X. Basagana, F. Ballester, C. Astrom, A. Paldy, M. Pascal, A. Gasparrini, et al. Synergistic effects of ambient temperature and air pollution on health in europe: results from the phase project. *International journal of environmental research and public health*, 15(9):1856, 2018.

- B. Armstrong, M. L. Bell, M. de Sousa Zanotti Stagliorio Coelho, Y.-L. Leon Guo, Y. Guo, P. Goodman, M. Hashizume, Y. Honda, H. Kim, E. Lavigne, et al. Longer-term impact of high and low temperature on mortality: an international study to clarify length of mortality displacement. *Environmental Health Perspectives*, 125(10):107009, 2017.
- S. Banerjee, B. P. Carlin, and A. E. Gelfand. *Hierarchical modeling and analysis for spatial data*. CRC press, 2014.
- S. Bergmann, B. Li, E. Pilot, R. Chen, B. Wang, and J. Yang. Effect modification of the short-term effects of air pollution on morbidity by season: A systematic review and meta-analysis. *Science of The Total Environment*, 716:136985, 2020.
- J. Besag. Spatial interaction and the statistical analysis of lattice systems. *Journal of the Royal Statistical Society: Series B (Methodological)*, 36(2):192–225, 1974.
- A. Bhaskar, J. Chandra, H. Hashemi, K. Butler, L. Bennett, J. Cellini, D. Braun, and F. Dominici. A literature review of the effects of air pollution on covid-19 health outcomes worldwide: Statistical challenges and data visualization. *Annual Review of Public Health*, 44:1–20, 2023.
- K. Bhaskaran, A. Gasparrini, S. Hajat, L. Smeeth, and B. Armstrong. Time series regression studies in environmental epidemiology. *International journal of epidemiology*, 42(4):1187–1195, 2013.
- A. Bitto and S. Frühwirth-Schnatter. Achieving shrinkage in a time-varying parameter model framework. *Journal of Econometrics*, 210(1):75–97, 2019.
- P. J. Brown, N. D. Le, and J. V. Zidek. Inference for a covariance matrix. *Aspects of uncertainty: a tribute to DV Lindley*, pages 77–92, 1994.
- B. Brunekreef, G. Downward, F. Forastiere, U. Gehring, D. Heederik, G. Hoek, M. Koopmans, L. Smit, and R. Vermeulen. Air pollution and covid-19: Including elements of air pollution in rural areas, indoor air pollution and vulnerability and resilience aspects of our society against respiratory disease, social inequality stemming from air pollution. *Study for the committee on Environment, Public Health and Food Safety, Policy Department for Economic, Scientific and Quality of Life Policies, European Parliament*, PE 658.216, 2021a. URL [https://www.europarl.europa.eu/thinktank/en/document/IPOL_STU\(2021\)658216](https://www.europarl.europa.eu/thinktank/en/document/IPOL_STU(2021)658216).
- B. Brunekreef, M. Strak, J. Chen, Z. J. Andersen, R. Atkinson, M. Bauwelinck, T. Bellander, M.-C. Boutron, J. Brandt, I. Carey, et al. Mortality and morbidity effects of long-term exposure to low-level pm2.5, bc, no2, and o3: an analysis of european cohorts in the elapse project. *Research Reports: Health Effects Institute*, 2021, 2021b.
- C3S. Era5 hourly data on single levels from 1940 to present. *Copernicus Climate Change Service (C3S) Climate Data Store (CDS)*, 2023. doi: 10.24381/cds.adbb2d47. Accessed on 22-03-2023.
- CAMS. European air quality reanalyses. *Copernicus Atmosphere Monitoring Service (CAMS) Atmosphere Data Store (ADS)*, 2023. URL <https://ads.atmosphere.copernicus.eu/cdsapp#!/dataset/cams-europe-air-quality-reanalyses?tab=overview>. Accessed on 22-03-2023.

- J. C. Chan and I. Jeliaskov. Efficient simulation and integrated likelihood estimation in state space models. *International Journal of Mathematical Modelling and Numerical Optimisation*, 1(1-2): 101–120, 2009.
- R. Chen, R. D. Peng, X. Meng, Z. Zhou, B. Chen, and H. Kan. Seasonal variation in the acute effect of particulate air pollution on mortality in the china air pollution and health effects study (capes). *Science of the total environment*, 450:259–265, 2013.
- M. Chiogna and C. Gaetan. Dynamic generalized linear models with application to environmental epidemiology. *Journal of the Royal Statistical Society Series C: Applied Statistics*, 51(4):453–468, 2002.
- M. Cork, D. Mork, and F. Dominici. Methods for estimating the exposure-response curve to inform the new safety standards for fine particulate matter. *arXiv preprint arXiv:2306.03011*, 2023.
- N. Cressie and C. K. Wikle. *Statistics for spatio-temporal data*. John Wiley & Sons, 2015.
- L. Dai, A. Zanobetti, P. Koutrakis, and J. D. Schwartz. Associations of fine particulate matter species with mortality in the united states: a multicity time-series analysis. *Environmental health perspectives*, 122(8):837–842, 2014.
- Q. Di, L. Dai, Y. Wang, A. Zanobetti, C. Choirat, J. D. Schwartz, and F. Dominici. Association of short-term exposure to air pollution with mortality in older adults. *Journal of the American Medical Association*, 318(24):2446–2456, 2017.
- F. Dominici, M. Daniels, S. L. Zeger, and J. M. Samet. Air pollution and mortality: estimating regional and national dose-response relationships. *Journal of the American Statistical Association*, 97(457):100–111, 2002.
- F. Dominici, A. Zanobetti, J. Schwartz, D. Braun, B. Sabath, and X. Wu. Assessing adverse health effects of long-term exposure to low levels of ambient air pollution: Implementation of causal inference methods. *Research Reports: Health Effects Institute*, 2022(211):1–56, 2022.
- M. Franklin, P. Koutrakis, and J. Schwartz. The role of particle composition on the association between pm2.5 and mortality. *Epidemiology*, 19(5):680, 2008.
- D. Gamerman and H. F. Lopes. *Markov chain Monte Carlo: stochastic simulation for Bayesian inference*. CRC press, 2006.
- D. Gamerman, L. Ippoliti, and P. Valentini. A dynamic structural equation approach to estimate the short-term effects of air pollution on human health. *Journal of the Royal Statistical Society Series C: Applied Statistics*, 71(3):739–769, 2022.
- A. E. Gelfand, H.-J. Kim, C. Sirmans, and S. Banerjee. Spatial modeling with spatially varying coefficient processes. *Journal of the American Statistical Association*, 98(462):387–396, 2003.
- A. Gelman. Inference and monitoring convergence. *Chapter in Gilks, Richardson, and Spiegelhalter (1996)*, 1996.
- A. Gelman and C. R. Shalizi. Philosophy and the practice of bayesian statistics. *British Journal of Mathematical and Statistical Psychology*, 66(1):8–38, 2013.

- A. Gelman, J. B. Carlin, H. S. Stern, D. B. Dunson, A. Vehtari, and D. B. Rubin. *Bayesian data analysis, third edition*. CRC Press, Nov 2013. ISBN 9781439898208.
- C. W. Granger. Non-linear models: Where do we go next-time varying parameter models? *Studies in Nonlinear Dynamics & Econometrics*, 12(3), 2008.
- S. Greven, F. Dominici, and S. Zeger. An approach to the estimation of chronic air pollution effects using spatio-temporal information. *Journal of the American Statistical Association*, 106(494): 396–406, 2011.
- H. Hao, Y. Wang, Q. Zhu, H. Zhang, A. Rosenberg, J. Schwartz, H. Amini, A. van Donkelaar, R. Martin, P. Liu, et al. National cohort study of long-term exposure to pm2.5 components and mortality in medicare american older adults. *Environmental Science & Technology*, 57(17): 6835–6843, 2023.
- H. Hersbach, B. Bell, P. Berrisford, G. Biavati, A. Horányi, J. Muñoz Sabater, J. Nicolas, C. Peubey, R. Radu, I. Rozum, et al. ERA5 hourly data on single levels from 1940 to present. *Copernicus Climate Change Service (C3S) Climate Data Store (CDS)*, 2018. doi: 10.24381/cds.adbb2d47. Accessed on 22-03-2023.
- J. S. Hodges and B. J. Reich. Adding spatially-correlated errors can mess up the fixed effect you love. *The American Statistician*, 64(4):325–334, 2010.
- INERIS, Aarhus University, MET Norway, IEK, IEP-NRI KNMI, METEO FRANCE, TNO, SMHI, et al. CAMS European air quality forecasts, ENSEMBLE data. *Copernicus Atmosphere Monitoring Service (CAMS) Atmosphere Data Store (ADS)*, 2022. URL <https://ads.atmosphere.copernicus.eu/cdsapp#!/dataset/cams-europe-air-quality-reanalyses?tab=overview>. Accessed on 22-03-2023.
- ISTAT. Decessi e cause di morte: cosa procude l’istat, 2023a. URL <https://www.istat.it/it/archivio/240401>. Istituto Nazionale di Statistica. Accessed on 22-03-2023.
- ISTAT. Tavole di mortalità: Classi di età, 2023b. URL http://dati.istat.it/Index.aspx?DataSetCode=DCIS_MORTALITA1. Istituto Nazionale di Statistica. Accessed on 20-03-2023.
- ISTAT. Popolazione residente al 1° gennaio, 2023c. URL http://dati.istat.it/Index.aspx?DataSetCode=DCIS_POPRES1. Istituto Nazionale di Statistica. Accessed on 22-03-2023.
- H. Janes, F. Dominici, and S. L. Zeger. Trends in air pollution and mortality: an approach to the assessment of unmeasured confounding. *Epidemiology*, pages 416–423, 2007.
- J. S. Ji, L. Liu, J. Zhang, H. Kan, B. Zhao, K. G. Burkart, and Y. Zeng. No2 and pm2. 5 air pollution co-exposure and temperature effect modification on pre-mature mortality in advanced age: a longitudinal cohort study in china. *Environmental Health*, 21(1):97, 2022.
- Z. Jing, P. Liu, T. Wang, H. Song, J. Lee, T. Xu, and Y. Xing. Effects of meteorological factors and anthropogenic precursors on pm2.5 concentrations in cities in china. *Sustainability*, 12(9): 3550, 2020.

- F. J. Kelly and J. C. Fussell. Size, source and chemical composition as determinants of toxicity attributable to ambient particulate matter. *Atmospheric environment*, 60:504–526, 2012.
- J. O. Klompmaker, F. Laden, P. James, M. B. Sabath, X. Wu, J. Schwartz, F. Dominici, A. Zanobetti, and J. E. Hart. Effects of long-term average temperature on cardiovascular disease hospitalizations in an american elderly population. *Environmental research*, 216:114684, 2023.
- J. K. Kodros, K. O’Dell, J. M. Samet, C. L’Orange, J. R. Pierce, and J. Volckens. Quantifying the health benefits of face masks and respirators to mitigate exposure to severe air pollution. *GeoHealth*, 5(9):e2021GH000482, 2021.
- D. Lee and G. Shaddick. Modelling the effects of air pollution on health using bayesian dynamic generalised linear models. *Environmetrics*, 19(8):785–804, 2008.
- J. Li, A. Woodward, X.-Y. Hou, T. Zhu, J. Zhang, H. Brown, J. Yang, R. Qin, J. Gao, S. Gu, et al. Modification of the effects of air pollutants on mortality by temperature: a systematic review and meta-analysis. *Science of the total environment*, 575:1556–1570, 2017.
- C. Liu, R. Chen, F. Sera, A. M. Vicedo-Cabrera, Y. Guo, S. Tong, E. Lavigne, P. M. Correa, N. V. Ortega, S. Achilleos, et al. Interactive effects of ambient fine particulate matter and ozone on daily mortality in 372 cities: two stage time series analysis. *The British Medical Journal*, 383, 2023.
- H. Lütkepohl. *New introduction to multiple time series analysis*. Springer Science & Business Media, 2005.
- P. Masselot, F. Sera, R. Schneider, H. Kan, É. Lavigne, M. Stafoggia, A. Tobias, H. Chen, R. T. Burnett, J. Schwartz, et al. Differential mortality risks associated with pm2.5 components: a multi-country, multi-city study. *Epidemiology*, 33(2):167–175, 2022.
- T. Nawrot, R. Torfs, F. Fierens, S. De Henauw, P. Hoet, G. Van Kersschaever, G. De Backer, and B. Nemery. Stronger associations between daily mortality and fine particulate air pollution in summer than in winter: evidence from a heavily polluted region in western europe. *Journal of Epidemiology & Community Health*, 61(2):146–149, 2007.
- C. J. Paciorek. The importance of scale for spatial-confounding bias and precision of spatial regression estimators. *Statistical Science*, 25(1):107, 2010.
- R. D. Peng and F. Dominici. Statistical methods for environmental epidemiology with r. *R: a case study in air pollution and health*, 2008.
- R. D. Peng, F. Dominici, R. Pastor-Barriuso, S. L. Zeger, and J. M. Samet. Seasonal analyses of air pollution and mortality in 100 us cities. *American journal of epidemiology*, 161(6):585–594, 2005.
- R. D. Peng, F. Dominici, and T. A. Louis. Model choice in time series studies of air pollution and mortality. *Journal of the Royal Statistical Society: Series A (statistics in society)*, 169(2): 179–203, 2006.

- G. Petris, S. Petrone, and P. Campagnoli. *Dynamic linear models with R*. Springer Science & Business Media, 2009.
- M. O. Prates, D. K. Dey, M. R. Willig, and J. Yan. Transformed gaussian markov random fields and spatial modeling of species abundance. *Spatial Statistics*, 14:382–399, 2015.
- M. O. Prates, D. R. Azevedo, Y. C. MacNab, and M. R. Willig. Non-separable spatio-temporal models via transformed multivariate gaussian markov random fields. *Journal of the Royal Statistical Society Series C: Applied Statistics*, 71(5):1116–1136, 2022.
- X. Qiu, M. Danesh-Yazdi, Y. Wei, Q. Di, A. Just, A. Zanobetti, M. Weisskopf, F. Dominici, and J. Schwartz. Associations of short-term exposure to air pollution and increased ambient temperature with psychiatric hospital admissions in older adults in the usa: a case–crossover study. *The Lancet Planetary Health*, 6(4):e331–e341, 2022.
- B. J. Reich, J. S. Hodges, and V. Zadnik. Effects of residual smoothing on the posterior of the fixed effects in disease-mapping models. *Biometrics*, 62(4):1197–1206, 2006.
- B. J. Reich, S. Yang, Y. Guan, A. B. Giffin, M. J. Miller, and A. Rappold. A review of spatial causal inference methods for environmental and epidemiological applications. *International Statistical Review*, 89(3):605–634, 2021.
- M. Renzi, S. Marchetti, F. De’Donato, M. Pappagallo, M. Scortichini, M. Davoli, L. Frova, P. Michelozzi, and M. Stafoggia. Acute effects of particulate matter on all-cause mortality in urban, rural, and suburban areas, italy. *International Journal of Environmental Research and Public Health*, 18(24):12895, 2021.
- W. J. Requia, A. M. Vicedo-Cabrera, H. Amini, and J. D. Schwartz. Short-term air pollution exposure and mortality in brazil: Investigating the susceptible population groups. *Environmental Pollution*, 340:122797, 2024.
- S. Roberts. Interactions between particulate air pollution and temperature in air pollution mortality time series studies. *Environmental research*, 96(3):328–337, 2004.
- S. K. Sahu. *Bayesian modeling of spatio-temporal data with R*. CRC Press, 2022.
- N. Siddika, A. K. Rantala, H. Antikainen, H. Balogun, A. K. Amegah, N. R. Ryti, J. Kukkonen, M. Sofiev, M. S. Jaakkola, and J. J. Jaakkola. Synergistic effects of prenatal exposure to fine particulate matter (pm_{2.5}) and ozone (o₃) on the risk of preterm birth: A population-based cohort study. *Environmental research*, 176:108549, 2019.
- M. Stafoggia, J. Schwartz, F. Forastiere, and C. Perucci. Does temperature modify the association between air pollution and mortality? a multicity case-crossover analysis in italy. *American journal of epidemiology*, 167(12):1476–1485, 2008.
- D. A. Stephens, W. S. Nobre, E. E. Moodie, and A. M. Schmidt. Causal inference under misspecification: Adjustment based on the propensity score (with discussion). *Bayesian Analysis*, 18(2):639–694, 2023.

- S. Sun, P. Cao, K.-P. Chan, H. Tsang, C.-M. Wong, and T.-Q. Thach. Temperature as a modifier of the effects of fine particulate matter on acute mortality in hong kong. *Environmental Pollution*, 205:357–364, 2015.
- L. Tian, F. Liang, Q. Guo, S. Chen, S. Xiao, Z. Wu, X. Jin, and X. Pan. The effects of interaction between particulate matter and temperature on mortality in beijing, china. *Environmental Science: Processes & Impacts*, 20(2):395–405, 2018.
- A. Vinson, A. Sidwell, O. Black, and C. Roper. Seasonal variation in the chemical composition and oxidative potential of pm2.5. *Atmosphere*, 11(10):1086, 2020.
- J. Wakefield. Disease mapping and spatial regression with count data. *Biostatistics*, 8(2):158–183, 2007.
- H. Walton, D. Evangelopoulos, M. Kasdagli, L. Selley, D. Dajnak, and K. Katsouyanni. Investigating links between air pollution, covid-19 and lower respiratory infectious diseases. *Research Report of the Environmental Research Group, Imperial College London*, 2021. URL <https://www.imperial.ac.uk/school-public-health/environmental-research-group/research/air-pollution-epidemiology/air-pollution-and-covid-19/>.
- M. West and J. Harrison. *Bayesian Forecasting and Dynamic Models*. Springer Series in Statistics. Springer-Verlag, New York, 1997. ISBN 9780387947259. doi: 10.1007/b98971.
- S. N. Wood. *Generalized additive models: an introduction with R*. CRC press, 2017.
- X. Wu, D. Braun, J. Schwartz, M. Kioumourtzoglou, and F. Dominici. Evaluating the impact of long-term exposure to fine particulate matter on mortality among the elderly. *Science advances*, 6(29):eaba5692, 2020.
- A. Zanobetti and J. Schwartz. Mortality displacement in the association of ozone with mortality: an analysis of 48 cities in the united states. *American Journal of Respiratory and Critical Care Medicine*, 177(2):184–189, 2008.
- A. Zanobetti, M. P. Wand, J. Schwartz, and L. M. Ryan. Generalized additive distributed lag models: quantifying mortality displacement. *Biostatistics*, 1(3):279–292, 2000.
- S. L. Zeger, F. Dominici, A. McDermott, and J. M. Samet. Mortality in the medicare population and chronic exposure to fine particulate air pollution in urban centers (2000–2005). *Environmental Health Perspectives*, 116(12):1614–1619, 2008.
- S. S. Zhou, S. Lukula, C. Chiossone, R. W. Nims, D. B. Suchmann, and M. K. Ijaz. Assessment of a respiratory face mask for capturing air pollutants and pathogens including human influenza and rhinoviruses. *Journal of thoracic disease*, 10(3):2059, 2018.
- X. Zhou, K. Josey, L. Kamareddine, M. C. Caine, T. Liu, L. J. Mickley, M. Cooper, and F. Dominici. Excess of covid-19 cases and deaths due to fine particulate matter exposure during the 2020 wildfires in the united states. *Science advances*, 7(33):eabi8789, 2021.

Supplementary Materials

A Data Collection

We gather daily data to analyze the short-term association between $PM_{2.5}$ and all-cause mortality in Piemonte and Lombardia regions for people aged 65 or more. The data span the period between 2018 and 2022, and are collected at the health district (HD) level.

- **Mortality data.** All-cause mortality data are collected from the Italian National Institute of Statistics (ISTAT, 2023a) for each municipality in the two regions, and are then spatially aggregated to the HD level, which represents the areal unit. The spatial domain comprises $N = 117$ HDs where 84 belong to the Lombardia region and 33 to the Piemonte region. The municipality of Campione d’Italia is excluded from the analysis since it has a small area and the time series contains many zeroes. Since the data refer to five consecutive years, the temporal dimension is $T = 1826$.

For $i = 1, \dots, N$ and $t = 1, \dots, T$, the standardized mortality ratio (SMR) is calculated as the ratio between the observed number of deaths, Y_{it} , and the expected number of deaths, E_{it} . The latter is obtained by indirect standardization (Banerjee et al., 2014, Sahu, 2022) as follows. The resident population aged 65 or more represents the population at risk and is obtained from the Italian National Institute of Statistics for each year (ISTAT, 2023c). The population is stratified by age class (65–69, 70–74, 75–79, 80–84, 85–89, 90–94, or 95+ years) and gender (male or female). For each stratum $k = 1, \dots, K$, the mortality rate for the northwest Italy is retrieved from the Italian National Institute of Statistics for each year (ISTAT, 2023b). The expected counts are thus computed as follows:

$$E_{it} = \sum_{k=1}^K Pop_{itk} r_{tk},$$

where Pop_{itk} and r_{tk} are the population at risk and the mortality rate in the k -th stratum, respectively.

- **Exposure data.** Data on $PM_{2.5}$ concentrations (expressed in $\mu g/m^3$) are collected from the Copernicus Atmosphere Monitoring Service’s (CAMS) Atmosphere Data Store (CAMS, 2023, INERIS et al., 2022). Hourly data are available at a spatial resolution of $0.1^\circ \times 0.1^\circ$, so we use zonal statistics to aggregate the estimates to the HD level, and then average across time to obtain daily data. To evaluate the short-term effect of interest, a lag of one day is applied to the exposure’s time series.
- **Potential confounders.** Daily temperature, daily relative humidity, indicator variables for the days of the week, for national holidays and for lockdown periods are treated as potential

measured confounders. We gather satellite measurements of air temperature and dew-point temperature (both expressed in Kelvin degrees) from the ERA5 reanalyses dataset available at the Copernicus Climate Change Service’s (C3S) Climate Data Store (C3S, 2023, Hersbach et al., 2018). Relative humidity (RH) is calculated from air temperature ($Temp$) dew-point temperature (DT) using the August-Roche-Magnus approximation formula (Alduchov and Eskridge, 1996):

$$RH = 100 \times \exp\left(\frac{17.625 \times DT}{243.04 + DT} - \frac{17.625 \times Temp}{243.04 + Temp}\right).$$

These hourly data are spatially and temporally averaged, similarly to the exposure.

The lockdowns are defined as follows: the first period is from March 9, 2020, to May 3, 2020, the second one is from December 21, 2020, to January 15, 2021, and the third one from March 6, 2021, to April 25, 2021.

B Descriptive Statistics

Descriptive statistics on the SMR data in all HDs are reported in Table B.1. The average SMR is 1.28 and 1.18 in Lombardia and Piemonte, respectively, and the standard deviation is slightly higher in Lombardia (0.34) than in Piemonte (0.26).

Table B.1: Descriptive statistics of daily SMR across all HDs in 2018–2022. Q1, Q2, and Q3 stand for first, second, and third quartiles, respectively.

Region	Mean	SD	Min	Q1	Q2	Q3	Max
Lombardia	1.28	0.29	0.75	1.14	1.25	1.39	3.52
Piemonte	1.18	0.22	0.68	1.03	1.14	1.29	2.10
Overall	1.25	0.26	0.75	1.12	1.22	1.37	3.09

Descriptive statistics on $PM_{2.5}$ levels in all HDs during the whole study period are reported in Table B.2. The average daily $PM_{2.5}$ concentration is $18.21 \mu g/m^3$ (standard deviation = 10.36) over the entire spatial domain, but Lombardia is more polluted than Piemonte. Table B.2 also reports descriptive statistics of temperature and relative humidity. The average daily temperature is $284.91 K$ (7.60), while the average daily relative humidity is 91.76% (3.59). These are very similar to the region-specific values (not shown).

Finally, Table B.3 reports the annual death counts and annual averages of the daily SMR and daily $PM_{2.5}$ for each administrative region.

Table B.2: Descriptive statistics of daily PM_{2.5} concentrations, temperature, and relative humidity across all HDs in 2018–2022. Q1, Q2, and Q3 stand for first, second, and third quartiles, respectively.

Variable	Mean	SD	Min	Q1	Q2	Q3	Max
PM _{2.5} ($\mu\text{g}/\text{m}^3$)	18.21	10.36	2.32	10.49	15.20	24.12	63.07
Temperature (K)	284.91	7.60	265.15	278.17	284.68	292.02	301.59
Relative humidity (%)	91.76	3.59	79.55	89.43	92.12	94.54	98.43

Table B.3: Annual mortality counts, and annual averages of daily SMR and daily PM_{2.5} concentrations for Piemonte and Lombardia (2018–2022).

Variable	Region	Year				
		2018	2019	2020	2021	2022
Mortality Counts	Lombardia	89742	90613	123586	97365	101069
	Piemonte	48739	48479	60364	51202	53581
	Overall	138481	139092	183950	148567	154650
SMR	Lombardia	1.32	1.32	1.23	1.29	1.26
	Piemonte	1.20	1.20	1.16	1.18	1.17
	Overall	1.29	1.29	1.21	1.26	1.24
PM _{2.5} ($\mu\text{g}/\text{m}^3$)	Lombardia	18.56	20.41	18.36	19.42	20.30
	Piemonte	14.00	16.47	14.33	15.17	15.91
	Overall	17.27	19.30	17.22	18.22	19.06

C Details on Competing Models

The proposed DGLM is compared to several approaches from the literature. These are fitted under the Bayesian paradigm, and the general hierarchical structure is as follows, for $i = 1, \dots, N$ and $t = 1, \dots, T$:

$$\begin{aligned}
 Y_{it} | \vartheta_{it} &\sim \text{Poi}(\exp(\vartheta_{it})) \\
 \vartheta_{it} &= o_{it} + \mathbf{A}'_{it} \mathbf{a}_i + \varepsilon_{it}, \quad \varepsilon_{it} \stackrel{iid}{\sim} \mathcal{N}(0, \tau_\varepsilon^2) \\
 \mathbf{a}_i &\sim \mathcal{N}(\boldsymbol{\mu}_a, \boldsymbol{\Sigma}_a) \\
 \boldsymbol{\mu}_a &\sim \mathcal{N}(0, 10^6 \mathbf{I}_{p_a}) \\
 \boldsymbol{\Sigma}_a &\sim \mathcal{IW}(p_a + 1.1, 10^{-4} \mathbf{I}_{p_a}) \\
 \tau_\varepsilon^2 &\sim \mathcal{IG}(1, 2.1 \times 10^{-5})
 \end{aligned}$$

where \mathbf{A}_{it} is a p_a -dimensional vector of covariates (i.e., intercept, exposure and measured confounders) and \mathbf{a}_i is the corresponding vector of coefficients. The vector $\boldsymbol{\mu}_a$ is of main interest, specifically its element(s) corresponding to the overall exposure effect.

The specification of \mathbf{A}_{it} depends on the approach under consideration as listed below.

- *Null*: the model that does not account for unmeasured confounding, for which $\mathbf{A}_{it} = (1, X_{it}, {}^m \mathbf{Z}'_{it})'$. The regression coefficients are allowed to vary across areas but not in time.

- *GLMadj*: the model that includes smooth function of time, $h(t; df)$, modelled as a natural cubic spline with df degrees of freedom. Let \mathbf{B}_t denote the vector of basis functions evaluated at time t . Then, we define $\mathbf{A}_{it} = (1, X_{it}, {}^m\mathbf{Z}'_{it}, \mathbf{B}'_t)'$.
- *Dummy*: Dai et al. (2014), Klompmaker et al. (2023) assume that the long-term exposure–outcome association vary by season. Following also Chen et al. (2013), Peng et al. (2005), we may extend this approach to our setting by including interaction terms. Let D_{jt} indicate an indicator variable for the j -th calendar season, for $j = 1, \dots, 4$, that is:

$$D_{jt} = \begin{cases} 1 & \text{if the day } t \text{ is in the } j\text{-th season} \\ 0 & \text{otherwise} \end{cases}$$

Then, $\mathbf{A}_{it} = (1, X_{it}D_{1t}, \dots, X_{it}D_{4t}, {}^m\mathbf{Z}'_{it}, \mathbf{B}'_t)'$. Henceforth, the Dummy model is similar to GLMadj, but it also captures season-specific exposure effects.

- *Periodic*: the exposure effect is assumed to be a linear combination of trigonometric functions, as in Chen et al. (2013), Peng et al. (2005). In this case, $\mathbf{A}_{it} = (1, X_{it}, X_{it} \cos(2\pi t/365), X_{it} \sin(2\pi t/365), {}^m\mathbf{Z}'_{it}, \mathbf{B}'_t)'$.
- *JDZ*: the model proposed by Janes et al. (2007), where the local exposure effect is of interest, hence $\mathbf{A}_{it} = (1, X_{it} - \widehat{X}_t, \widehat{X}_t, {}^m\mathbf{Z}'_{it}, \mathbf{B}'_t)'$. Here, \widehat{X}_t denotes the overall temporal trend (see also Section 3), and \mathbf{B}_t^* denotes the vector of basis functions from a natural cubic spline with $df - 1$ degrees of freedom, evaluated at time t .

The unknown function $h(\cdot; \cdot)$ is modelled as a natural cubic spline of time with 8 degrees of freedom per year (so $df = 40$), and is used to control for unmeasured confounding. The overall trend, \widehat{X}_t , is obtained as the fitted values of a regression of X_{it} on a natural cubic spline of time with 4 degrees of freedom per year. Bases from natural cubic splines of temperature (with 7 degrees of freedom) and of relative humidity (with 4 degrees of freedom) are included as measured confounders. ${}^m\mathbf{Z}_{it}$ also includes the indicator variables for the day of the week, for holidays, and for the lockdown periods.

D Posterior Full Conditional Distributions for the Proposed DGLM

We provide the computational details to make inference on the model proposed in Section 3 and following the discussion in Section 4 of the main manuscript. In particular, stacking Equation (7) of the main text over the T time instants, we have (see also Chan and Jeliaskov, 2009):

$$\boldsymbol{\vartheta} = \mathbf{o} + \mathbf{G}\boldsymbol{\gamma} + \tilde{\mathbf{u}},$$

E Additional Details on Simulation Study 1

E.1 Data Generation Mechanism

To simulate the variables, we use the following data generation mechanism. The spatial domain comprises $N = 100$ contiguous HDs, while the temporal dimension is set to $T = 300$. Let $\mathbf{X} = (\mathbf{X}_1, \dots, \mathbf{X}_T)'$, with $\mathbf{X}_t = (X_{1t}, \dots, X_{Nt})'$, $t = 1, \dots, T$, be the exposure, and let $\mathbf{Z} = (\mathbf{Z}_1, \dots, \mathbf{Z}_T)'$, with $\mathbf{Z}_t = (Z_{1t}, \dots, Z_{Nt})'$, $t = 1, \dots, T$, be the unmeasured confounder. It is thus assumed that

$$\begin{bmatrix} \mathbf{X} \\ \mathbf{Z} \end{bmatrix} \sim \mathcal{N} \left(\begin{bmatrix} \boldsymbol{\mu}_x \\ \boldsymbol{\mu}_z \end{bmatrix}, \begin{bmatrix} \boldsymbol{\Sigma}_x & \boldsymbol{\Sigma}_{xz} \\ \boldsymbol{\Sigma}_{zx} & \boldsymbol{\Sigma}_z \end{bmatrix} \right), \quad (9)$$

where $\boldsymbol{\mu}_x$ and $\boldsymbol{\mu}_z$ are the spatio-temporal means generated from Fourier basis expansions such that their correlation is approximately 0.5. It is assumed that the covariance matrices can be factorized as $\boldsymbol{\Sigma}_x = \boldsymbol{\Sigma}_x^{1/2} \boldsymbol{\Sigma}_x^{1/2'}$, $\boldsymbol{\Sigma}_z = \boldsymbol{\Sigma}_z^{1/2} \boldsymbol{\Sigma}_z^{1/2'}$, $\boldsymbol{\Sigma}_{xz} = \boldsymbol{\Sigma}'_{zx} = \rho_{xz} \boldsymbol{\Sigma}_x^{1/2} \boldsymbol{\Sigma}_z^{1/2'}$, and $\rho_{xz} = \text{Cor}(X_{it}, Z_{it})$, for $i = 1, \dots, N$, and $t = 1, \dots, T$.

We then assume that exposure and unmeasured confounder are spatial VAR(1) processes (Cressie and Wikle, 2015, Sahu, 2022). We now explain how $\boldsymbol{\Sigma}_x$ is parameterized, and the same applies to $\boldsymbol{\Sigma}_z$. If a stable VAR(1) model is assumed for the exposure where the temporal autocorrelation is controlled by a scalar, $\phi_x^T \in (0, 1)$, then it can be shown (see, for example, Lütkepohl, 2005, Section 2.1.4) that $\boldsymbol{\Sigma}_x = \boldsymbol{\Gamma}_{x,ar} \otimes \mathbf{C}_x(0)$, where

$$\mathbf{C}_x(0) = \mathbb{E} [\mathbf{X}_t \mathbf{X}_t'] = \frac{\tau_x^2}{1 - (\phi_x^T)^2} \boldsymbol{\Omega}_{x,pcar}^{-1}$$

indicates a zero-lag covariance matrix, and $\boldsymbol{\Gamma}_{x,ar}$ is the correlation matrix of a first-order autoregressive process with generic element $(\boldsymbol{\Gamma}_{x,ar})_{jk} = (\phi_x^T)^{|j-k|}$. The spatial dependence is defined by the matrix $\boldsymbol{\Omega}_{x,pcar}$, which has a proper conditional autoregressive (PCAR) specification (Banerjee et al., 2014, Besag, 1974, Sahu, 2022):

$$\boldsymbol{\Omega}_{x,pcar} = \mathbf{D}_w - \phi_x^S \mathbf{W}, \quad (10)$$

where \mathbf{D}_w is a diagonal matrix with the number of neighbors of each HD on the diagonal, \mathbf{W} is the binary adjacency matrix, and $\phi_x^S \in (0, 1)$ is the spatial autocorrelation parameter. \mathbf{W} is an $N \times N$ matrix with entries $w_{ij} = 1$ if areal units i and j share a border, and $w_{ij} = 0$ otherwise; also, $w_{ii} = 0$.

We set $\rho_{xz} = 0.5$, $\tau_x^2 = 4 \times 10^{-4}$, and $\tau_z^2 = 1 \times 10^{-3}$, and then use different values for the spatial and temporal autocorrelation parameters to define the scenarios in Table 1 of the main manuscript.

Once all the matrices in Equation (9) are defined, we simulate the exposure from its marginal distribution, then the unmeasured confounder from the conditional distribution $\mathbf{Z}|\mathbf{X} \sim \mathcal{N}(\boldsymbol{\mu}_{z|x}, \boldsymbol{\Sigma}_{z|x})$

where:

$$\begin{aligned}\boldsymbol{\mu}_{z|x} &= \mathbb{E}[\mathbf{Z}|\mathbf{X} = \mathbf{x}] = \boldsymbol{\mu}_z + \boldsymbol{\Sigma}_{zx}\boldsymbol{\Sigma}_x^{-1}(\mathbf{x} - \boldsymbol{\mu}_x), \\ \boldsymbol{\Sigma}_{z|x} &= \mathbb{V}\text{ar}[\mathbf{Z}|\mathbf{X} = \mathbf{x}] = \boldsymbol{\Sigma}_z - \boldsymbol{\Sigma}_{zx}\boldsymbol{\Sigma}_x^{-1}\boldsymbol{\Sigma}_{xz}.\end{aligned}$$

Finally, the outcome is generated using the following model:

$$Y_{it}|\mu_{it} \stackrel{ind}{\sim} \mathcal{Poi}(\mu_{it}) \tag{11}$$

$$\vartheta_{it} = o_{it} + \beta_{0i} + \beta_{1t}X_{it} + Z_{it} + u_{it}, \quad u_{it} \stackrel{iid}{\sim} \mathcal{N}(0, \tau_u^2), \tag{12}$$

where $\mu_{it} = \exp(\vartheta_{it})$, $o_{it} = \log(E_{it})$ is the offset term, and $\tau_u^2 = 10^{-5}$. The expected counts, E_{it} , are obtained by using the resident population aged ≥ 65 years and the age-specific standardized mortality rates of year 2018. The population and the rates are assumed to be constant in time.

E.2 Performance Assessment

To complete the results of Simulation Study 1, Table E.4 reports, for each scenario and model, the value for the three indices, namely:

- average mean squared error, $MSE_{avg} = \frac{1}{T} \sum_{t=1}^T \left[\frac{1}{100} \sum_{i=1}^{100} (\mathbb{E}[P_t|\bullet] - P_t)^2 \right]$
- maximum absolute bias, $MAB = \max_t |\mathbb{E}[P_t|\bullet] - P_t|$
- average mean absolute error, $MAE_{avg} = \frac{1}{T} \sum_{t=1}^T \left[\frac{1}{100} \sum_{i=1}^{100} |\mathbb{E}[P_t|\bullet] - P_t| \right]$

Here, the differences are computed with respect to P_t , i.e. the true simulated percent change of risk.

Table E.4 indicates that, if the exposure effect is constant, the GLMadj model should be preferred, otherwise the DGLM is the best choice. Note, however, that the shape of the exposure effect is not known in practice, so the DGLM is the most robust choice across all scenarios.

Table E.4: Simulation Study 1: MSE_{avg} , MAB , and MAE_{avg} calculated for each model considered under each Scenario. The lowest values are indicated in italic.

Scenario	Exposure Effect	MSE_{avg}			MAB			MAE_{avg}		
		DGLM	Null	GLMadj	DGLM	Null	GLMadj	DGLM	Null	GLMadj
S1	Constant	0.642	63.158	<i>0.368</i>	0.728	7.929	<i>0.568</i>	0.686	7.929	<i>0.568</i>
	Periodic	<i>0.697</i>	115.672	3.276	<i>0.833</i>	12.678	3.109	<i>0.717</i>	10.643	1.490
	Complex	<i>0.672</i>	66.741	1.283	<i>1.217</i>	9.912	2.423	<i>0.691</i>	8.099	0.989
S2	Constant	6.886	19.741	<i>6.622</i>	3.660	4.435	<i>2.547</i>	2.571	4.435	<i>2.547</i>
	Periodic	<i>7.177</i>	32.742	10.620	<i>3.337</i>	7.566	4.935	<i>2.625</i>	5.531	2.900
	Complex	<i>6.782</i>	20.939	8.094	<i>3.691</i>	6.285	4.476	<i>2.547</i>	4.472	2.664
S3	Constant	0.251	45.706	<i>0.085</i>	0.406	6.760	<i>0.260</i>	0.331	6.760	<i>0.260</i>
	Periodic	<i>0.276</i>	86.516	2.706	<i>0.480</i>	11.224	2.823	<i>0.360</i>	9.189	1.396
	Complex	<i>0.271</i>	48.538	0.981	<i>0.911</i>	8.717	2.126	<i>0.325</i>	6.904	0.852

E.3 On The Removal of Large-Scale Temporal Trend

We argue that the term $X_{it} - \widehat{X}_t$, for $i = 1, \dots, N$ and $t = 1, \dots, T$, should be used in place of simply X_{it} in the DGLM. Removing the overall temporal trend from the exposure not only follows from theoretical arguments (see Equation (3) in the main paper), but also it is crucial to control for confounding bias. The local variations in the exposure are in fact less likely to be confounded by the unmeasured confounder, which is assumed to be spatially and temporally smooth (Greven et al., 2011, Janes et al., 2007) – see also Section 3 of the manuscript. To illustrate this with simulated data, we compare the proposed DGLM with a reparameterized model that does not remove the overall trend from the exposure. Essentially, Equation (6) in the paper can be rewritten as:

$$\vartheta_{it} = o_{it} + \beta_{0it}^* + \beta_{1t}X_{it} + {}^m\mathbf{Z}'_{it}\boldsymbol{\alpha}_m + \tilde{u}_{it},$$

where

$$\beta_{0it}^* = \beta_{0it} - \beta_{1t}\widehat{X}_t.$$

We refer to this model as *DGLM_single*, since it is a single-step approach that does not require to estimate the overall temporal trend.

The results, in terms of percent change of risk associated with a 10-unit increase in the exposure, P_t , for each scenario considered in the main paper are depicted in Figure E.1. The estimates tend to differ at the beginning and at the end of the time window, where the *DGLM_single* model is more biased. In addition, note that the *DGLM_single* model is not able to recover the constant effect in the top-left subplot. For completeness, Table E.5 reports the MSE_{avg} , MAB , and MAE_{avg} for both model considered under each scenario, where it is confirmed that the proposed DGLM outperforms the *DGLM_single* model in all cases.

Table E.5: Simulation Study 1: MSE_{avg} , MAB , and MAE_{avg} calculated for the DGLM and *DGLM_single* models under each Scenario. The lowest values for each index are indicated in *italic*.

Scenario	Exposure Effect	MSE_{avg}		MAB		MAE_{avg}	
		DGLM	<i>DGLM_single</i>	DGLM	<i>DGLM_single</i>	DGLM	<i>DGLM_single</i>
S1	Constant	<i>0.642</i>	0.873	<i>0.728</i>	2.002	<i>0.686</i>	0.773
	Periodic	<i>0.697</i>	0.816	<i>0.833</i>	1.762	<i>0.717</i>	0.763
	Complex	<i>0.672</i>	0.890	<i>1.217</i>	1.955	<i>0.691</i>	0.799
S2	Constant	<i>6.886</i>	7.711	<i>3.660</i>	4.351	<i>2.571</i>	2.707
	Periodic	<i>7.177</i>	7.695	<i>3.337</i>	4.178	<i>2.625</i>	2.706
	Complex	<i>6.782</i>	7.454	<i>3.691</i>	4.333	<i>2.547</i>	2.660
S3	Constant	<i>0.251</i>	0.254	<i>0.406</i>	1.033	<i>0.406</i>	0.418
	Periodic	0.276	<i>0.250</i>	<i>0.480</i>	0.957	0.428	<i>0.417</i>
	Complex	<i>0.271</i>	0.282	<i>0.911</i>	1.183	<i>0.418</i>	0.436

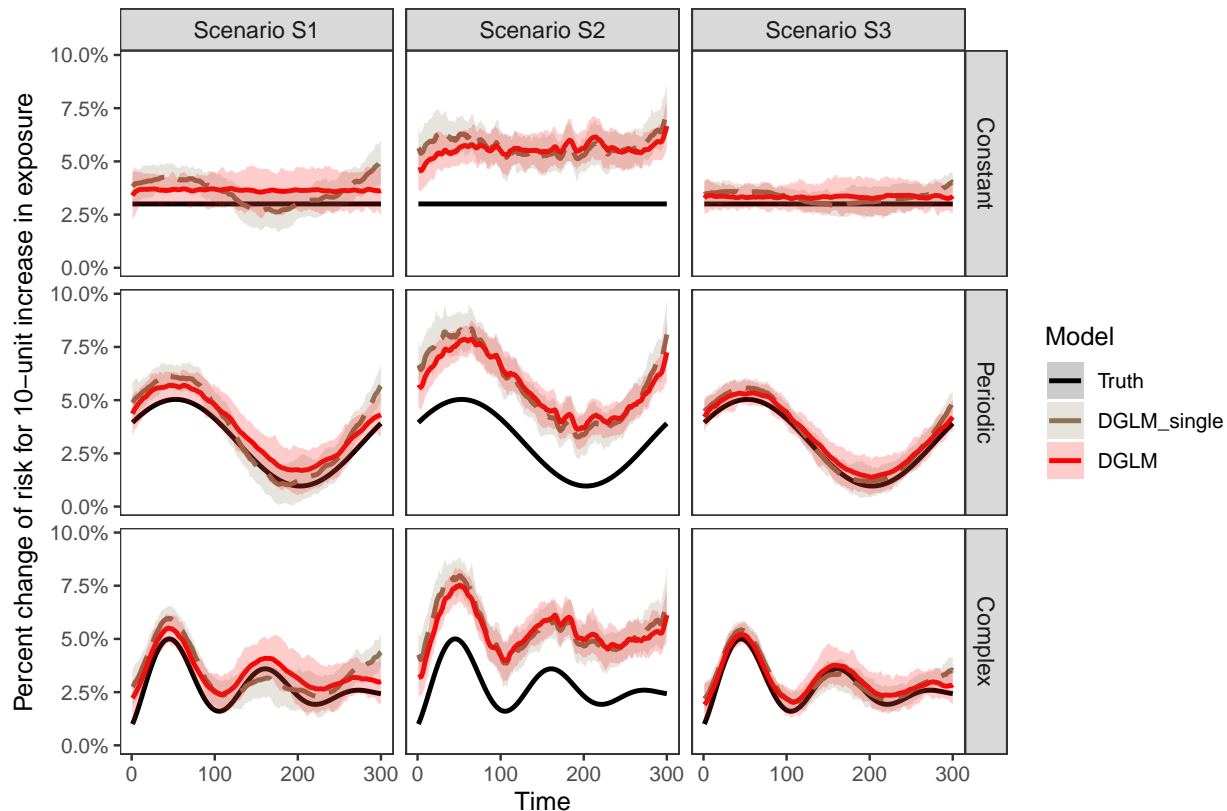


Figure E.1: Simulation Study 1: results are expressed in terms of percent change of risk associated with a 10-unit increase in the exposure, P_t . The black line represents the true exposure effect (whose shape differs in each row). The solid red and dashed brown lines represent the average of the posterior means of P_t obtained from DGLM and DGLM_no over 100 replicates, respectively. The shaded areas represent the percentiles 2.5 and 97.5 of the posterior means of P_t under each approach.

F Simulation Study 2

We now illustrate *Simulation Study 2*, where we want to assess whether the proposed DGLM is able to recover the first derivative of the unknown functional form, which represents the marginal effect of the exposure on the outcome. To this end, we consider Scenarios S1 and S2 again, but we assume that the linear predictor is as follows:

$$\vartheta_{it} = o_{it} + \beta_{0i} + f(X_{it}; \gamma_f) + Z_{it} + u_{it},$$

where $f(X_{it}; \gamma_f) = \gamma_{f0} + \gamma_{f1}X_{it} + \gamma_{f2}X_{it}^2$, $\gamma_{f0} = \gamma_{f1} = 0$, $\gamma_{f2} = 2.5 \times 10^{-5}$. Henceforth, the true values of the time-varying coefficients are $\beta_{1t} = 5 \times 10^{-5}\widehat{X}_t$, and $\beta_{0it} = \beta_{0i} + 2.5 \times 10^{-5}\widehat{X}_t^2 + Z_{it}$. All the other parameters are the same as in the previous Section.

Scenario S1. Figure F.2 refers to Scenario S1 and consists of two subplots. The top subplot compares spatial averages of the time-varying intercepts. That is,

$$\overline{\beta_{0t}} = \frac{1}{N} \sum_{i=1}^N \beta_{0it} \quad \text{for } t = 1, \dots, T$$

and

$$\overline{\mathbb{E}[\beta_{0t}|\bullet]} = \frac{1}{N} \sum_{i=1}^N \mathbb{E}[\beta_{0it}|\bullet] \quad \text{for } t = 1, \dots, T$$

denote the average true intercept and average posterior mean, respectively. These quantities are different across the 100 replicates, so the blue (green) line corresponds to the average $\overline{\beta_{0t}}$ ($\overline{\mathbb{E}[\beta_{0t}|\bullet]}$), while the shaded area of the same color defines the percentiles 2.5 and 97.5. The blue and green shaded areas do not completely overlap, hence the unmeasured confounder can be captured only in part. The bottom subplot shows that the true value of β_{1t} (black line) is almost always within the red shaded area, indicating that confounding bias is alleviated but not completely ruled out.

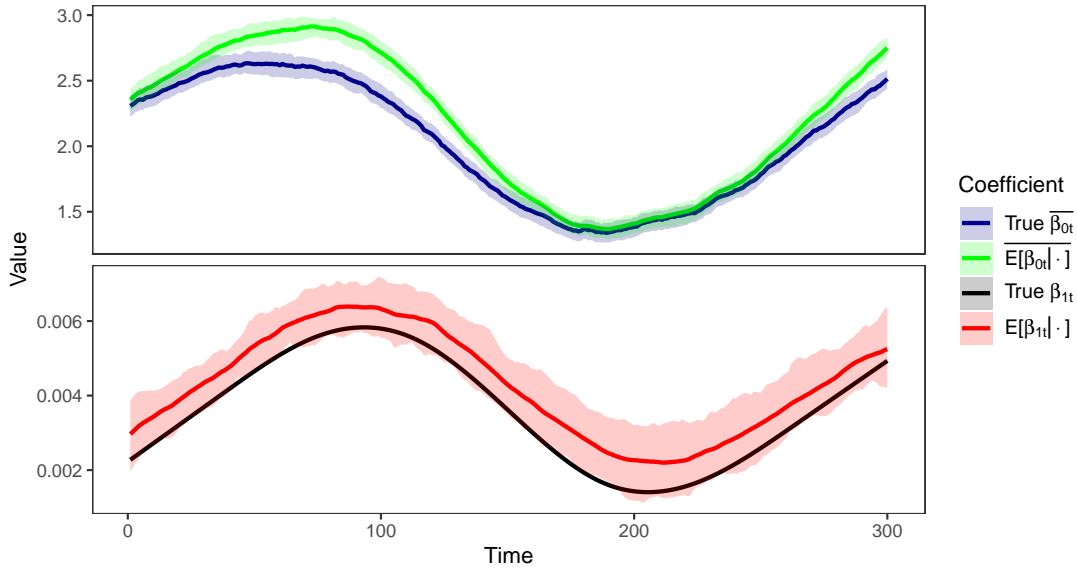


Figure F.2: Simulation Study 2: results from Scenario S1 with $f(X_{it}; \gamma_f) = \gamma_{f0} + \gamma_{f1}X_{it} + \gamma_{f2}X_{it}^2$. Top: the blue solid line and the blue shaded area are the average and the percentiles 2.5 and 97.5 of the spatial mean of the simulated intercepts over 100 replicated datasets; the green solid line and green shaded area depict the same quantities but for the corresponding spatially-averaged posterior mean obtained from the proposed DGLM. Bottom: the black solid line represents the true exposure effect, while the red solid line and the shaded area represent the average and the percentiles 2.5 and 97.5 of the posterior means of β_{1t} .

Scenario S2. As for Scenario S2, Figure F.3 indicates that it is not possible to completely recover the true function, $f(\cdot; \cdot)$. The unmeasured confounder has low temporal autocorrelation, and the

posterior means of the intercepts tend to have a rougher behavior. However, some variation in the unmeasured confounder is “absorbed” by the local exposure effect, which remains biased.

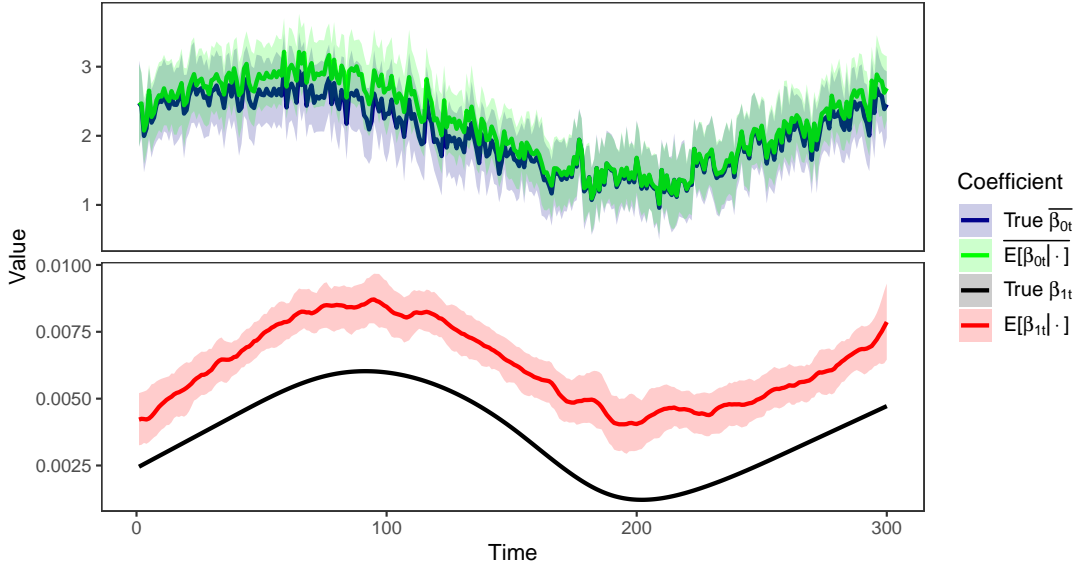


Figure F.3: Simulation Study 2: results from Scenario S2 with $f(X_{it}; \gamma_f) = \gamma_{f0} + \gamma_{f1}X_{it} + \gamma_{f2}X_{it}^2$. Top: the blue solid line and the blue shaded area are the average and the percentiles 2.5 and 97.5 of the spatial mean of the simulated intercepts over 100 replicated datasets; the green solid line and green shaded area depict the same quantities but for the corresponding spatially-averaged posterior mean obtained from the proposed DGLM. Bottom: the black solid line represents the true exposure effect, while the red solid line and the shaded area represent the average and the percentiles 2.5 and 97.5 of the posterior means of β_{1t} .

Scenario without confounding. To understand whether the residual bias in Figures F.2 and F.3 is due to the Taylor’s approximation, we now assume that the outcome is not affected by any confounder, i.e. $\mathbf{Z} = \mathbf{0}$. We only report the results for the Scenario S1 where $\phi_x^S = \phi_x^T = 0.2$. The estimated exposure effect is depicted in Figure F.4, which indicates that the proposed DGLM is able to recover the true effect, with no visible difference between the black and red lines for almost all the temporal domain.

G Application: Comparison with Restricted Model

We assess the impact that imposing some constraints on the proposed DGLM has on the estimated exposure effect. Specifically, we remove the measured confounders from the model specification. This is equivalent to imposing that $\alpha_m = \mathbf{0}$ in Equation (6) of the main text. Hence, the linear

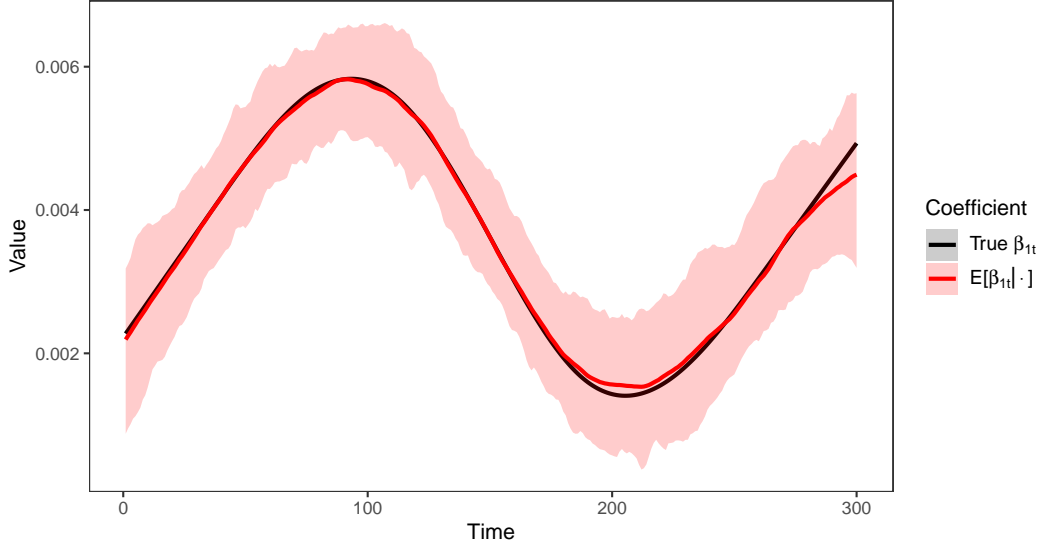


Figure F.4: Simulation Study 2: results from Scenario S1 without confounding. The black solid line represents the true exposure effect. The red solid line and the shaded area represent the average and the percentiles 2.5 and 97.5 of the posterior means of β_{1t} obtained from the proposed DGLM over 100 replicated datasets.

predictor and the temporal dynamics of the coefficients are specified as follows:

$$\begin{aligned}\boldsymbol{\vartheta}_t &= \boldsymbol{\alpha}_t + \tilde{\mathbf{X}}_t \tilde{\boldsymbol{\beta}}_t + \tilde{\mathbf{u}}_t, \\ \tilde{\boldsymbol{\beta}}_t &= \tilde{\boldsymbol{\beta}}_{t-1} + \tilde{\mathbf{w}}_t.\end{aligned}$$

We refer to the implied model as DGLM-X to emphasize that the exposure is the only covariate. Figure G.5 shows the posterior mean of the percent change of risk, as defined above, under the DGLM-X (in green) and the proposed DGLM (in red). It suggests that, in general, the temporal dynamic of the exposure effect would not be affected much if the measured confounders were not included in the model. Henceforth, the proposed DGLM can provide accurate estimates even in complex scenarios.

However, it is worth noting that the DGLM-X provides greater estimates than the proposed estimates during the summer, while during the winter the estimates are quite similar. This suggests that the confounding effect may vary across time. We hypothesize that this is due to air temperature that exceeds a certain threshold; in other words, confounding may occur due to heat waves. In fact, heat waves are demonstrated to have an increased effect on mortality during summer days with relatively high levels of PM_{2.5} concentrations, and this positive correlation may be the source of the overestimation (Analitis et al., 2008, 2014). Another study observed a similar result for the population aged 75 years or more (Analitis et al., 2018). Another possible explanation for the overestimation could be the modification of the PM_{2.5} chemical composition, with high levels of the most toxic compounds developing in summer (Vinson et al., 2020).

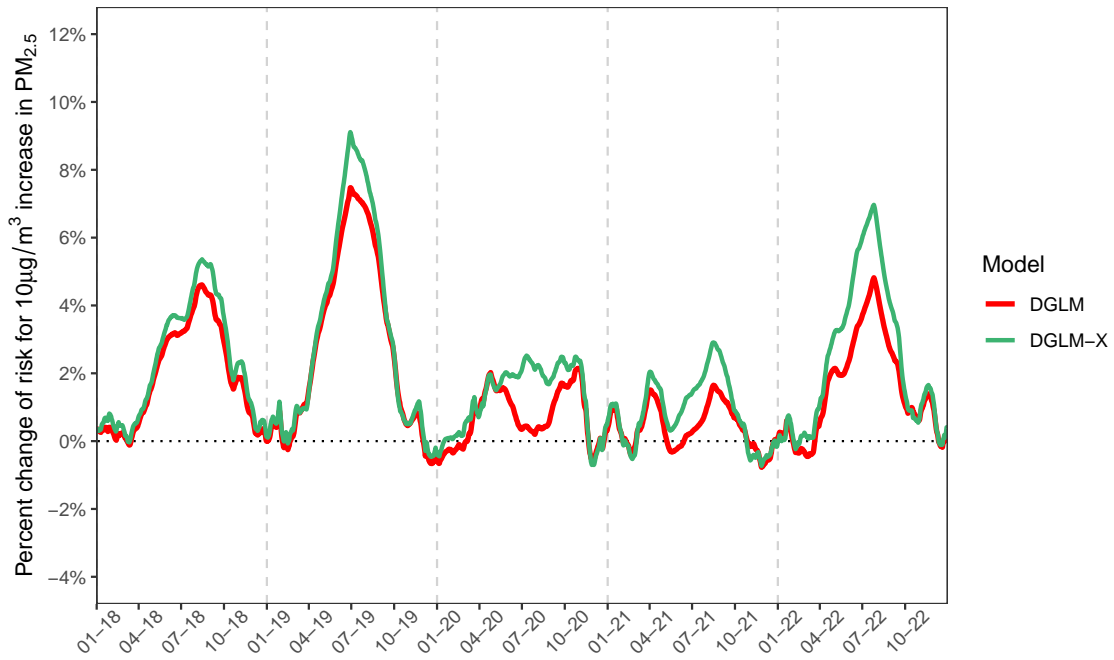


Figure G.5: Estimated time-varying percent change of risk associated with a $10 \mu\text{g}/\text{m}^3$ increase in the $\text{PM}_{2.5}$ concentrations. The red line represents the posterior mean of the proposed DGLM, while the green line the posterior mean of the DGLM-X.